geosciences

Article

Metamorphic Conditions and Raman Spectroscopic Carbonaceous Material Thermometry of Host Schists of Olympiada and Eldorado Gold Deposits (Yenisey Ridge, Russia)

Vasiliy Sukhorukov [1,2,*], Valeriya Volkova [1], Peter Nevolko [1,2] and Pavel Kozlov [3]

1 Sobolev Institute of Geology and Mineralogy, Siberian Branch of Russian Academy of Sciences, Koptyuga Av. 3, 630090 Novosibirsk, Russia; v.volkova@g.nsu.ru (V.V.); nevolko@igm.nsc.ru (P.N.)
2 Department of Geology and Geophysics, Novosibirsk State University, Pirogova Str. 2, 630090 Novosibirsk, Russia
3 Zavaritskii Institute of Geology and Geochemistry, Ural Branch of the Russian Academy of Sciences, 7 Per. Pochtovii, 620151 Ekaterinburg, Russia; geoeco2012@yandex.ru
* Correspondence: svp@igm.nsc.ru

Abstract: Metamorphic processes play a key role in forming orogenic gold deposits. In this paper, we present new evidence that host schists of the two largest gold deposits of the Yenisey ridge (Russia) Olympiada and Eldorado underwent a single stage of metamorphism in contrast to surrounding blocks. This metamorphism is of moderate thermal gradient and belongs to the Barrovian type, which is typical for the collisional event in the time range 800–850 Ma. The new Ar/Ar age data presented in this paper and the review of magmatic and metamorphic events and ore-forming processes indicate that the most productive stage (gold-sulfide-quartz) correlates well in time with the regional metamorphism of the Barrovian type. This indicates that metamorphic processes can have a crucial role in forming gold deposits of the Yenisey ridge. Carbonaceous material thermometry indicates a wide range of obtained temperatures around 90–150 °C around the mean temperature for each sample. The highest temperatures are close to the peak metamorphic temperatures estimated by garnet-biotite thermometry.

Keywords: Yenisey Ridge; metamorphism; gold deposits; Ar-Ar; Raman spectra; carbonaceous material

Citation: Sukhorukov, V.; Volkova, V.; Nevolko, P.; Kozlov, P. Metamorphic Conditions and Raman Spectroscopic Carbonaceous Material Thermometry of Host Schists of Olympiada and Eldorado Gold Deposits (Yenisey Ridge, Russia). *Geosciences* **2021**, *11*, 452. https://doi.org/10.3390/geosciences11110452

Academic Editors: Aberra Mogessie and Jesus Martinez-Frias

Received: 19 July 2021
Accepted: 28 October 2021
Published: 2 November 2021

1. Introduction

Metamorphic processes play a key role in forming orogenic gold deposits [1]. The genesis of many gold deposits with polygenic history, which included both metamorphic and magmatic processes, often remains debated. The controversy is due to difficulties in the interpretation of geochronological data for overlapping magmatic and metamorphic processes of different ages. The Yenisey ridge (Russia) is one such region with polygenic history. It is a Neoproterozoic accretionary-collisional orogen, extending for 700 km along the western margin of the Siberian craton situated between the craton to the east and West Siberian basin to the west. Most gold deposits occur in the lower part of the Sukhoi Pit Group, represented by clastic, carbonaceous, and calcareous clastic rocks of the Korda, Gorbilok, and Uderei Formations [2].

We present in this paper new data on pressure-temperature parameters of metamorphism of host schists of the two largest gold deposits of the Yenisey ridge, Olympiada and Eldorado and its tectonic and time correlation with metamorphic events around the whole orogen of the Yenisey ridge. New Ar-Ar data on ore formation of the Eldorado gold deposit allows correlating the ore-forming processes with Barrovian type collisional metamorphism.

Raman spectroscopy of organic carbonaceous material is used as a quantitative tool to decipher rocks' thermal history during metamorphism [3–5]. Graphitization is the temperature-dependent progressive transformation of carbonaceous material from amorphous to stable graphite structures. The degree of graphitization is considered to be a reliable indicator of metamorphic temperature [6,7]. Because graphitization is essentially irreversible, the structure of carbonaceous material records peak metamorphic conditions. Nevertheless, for many cases interpretation of carbonaceous thermometry is controversial. Here, we present the new data from Raman spectroscopy of carbonaceous material from the host schists of Olympiada and Eldorado gold deposits. Comparison with conventional geothermometry allows the conclusion that carbonaceous thermometry indicates reliable results in temperature intervals around 600 °C subject to the optimum number of analyzes.

2. Regional Geology and Metallogeny of the Yenisey Ridge

The Yenisey Ridge (YR) is a 200-km-wide Neoproterozoic accretionary-collisional orogen, extending for 700 km along the western margin of the Siberian craton (Figure 1). There are two segments in the orogen (South Yenisey and Trans-Angara), separated by the east-west transcrustal Angara fault (Figure 3). The southern part of YR is composed of Paleoproterozoic collisional complexes metamorphosed at conditions of high- and ultrahigh-temperature metamorphism in the time interval 1.86–1.75 Ga [8–10]. The northern segment consists of the East Angara, Central Angara, and Isakovka terranes, comprising mostly Meso- to Neoproterozoic rocks [11,12]. These terranes are separated by the Ishimba, Tatarka, Priyenisey, and Anikino regional faults, with the Tatarka-Ishimba zone of regional faults, representing a suture zone between the Central Angara and East Angara terranes (Figure 1). The majority of gold deposits occur in the eastern part of the Central Angara terrane. Metamorphosed Precambrian sedimentary rocks dominate the Trans-Angara segment. Gneiss and schist (Teya Group) are considered the oldest stratigraphic unit. It is overlain by Meso- to Neoproterozoic cyclical sedimentary sequences divided into Sukhoi Pit, Tungusik, Oslyan, Chingasan, and Taseevo Groups [13]. Most gold deposits occur in the lower part of the Sukhoi Pit Group, represented by clastic, carbonaceous, and calcareous clastic rocks of the Korda, Gorbilok, and Uderei Formations. Sazonov et al. [7] estimated that the Korda Formation hosts 73% of the discovered gold (Olympiada, Blagodatnoe, Titimukhta, Tyrada, Olenie and Panimba deposits). The Gorbilok and Uderei Formations host many gold deposits and occurrences but only account for 7% (Eldorado, Pervenets, Udarnyi) and 20% (Sovetskoe, Veduga, Bogolyubovskoe) of the known endowment, respectively.

Magmatic rocks are represented by numerous ultramafic to felsic intrusions, including some alkaline varieties. The most abundant granitoids can be grouped into two types of massifs: (1) 880 to 860 Ma syncollisional granitoids of the Teya and Eruda Complexes, and (2) 760 to 720 Ma syn- to post-collisional granitoids of the Ayakhta and Glushikha Complexes [14]. The youngest A-type granitoids, nepheline syenite, and carbonatite belong to the 650 to 630 Ma anorogenic Tatarka Complex, with associated rare metal and rare earth mineralization. Genetic relationships of the gold deposits and granitoid magmatism are debated [13,15–18].

Regional metamorphism of the Trans-Angara sedimentary formations varies from amphibolite and epidote-amphibolite facies in the lower part of the sequence (Teya Group) to greenschist facies in the bulk of the Sukhoi Pit and Tungusik Groups [11,12]. This regional metamorphic zonation is overprinted by contact metamorphic zones around late intrusions [19]. Two main metamorphic episodes can be found over the Trans-Angara part of YR. The first stage is high-gradient metamorphism (HT/LP type) and the second stage belongs to the moderate-gradient metamorphism of the Barrovian type. The age of the first episode is unclear, known age estimates fall into the range from 1015 to 850 Ma [20,21]. The age of the second (Barrovian-type) episode is estimated in the range 850–800 Ma [22,23].

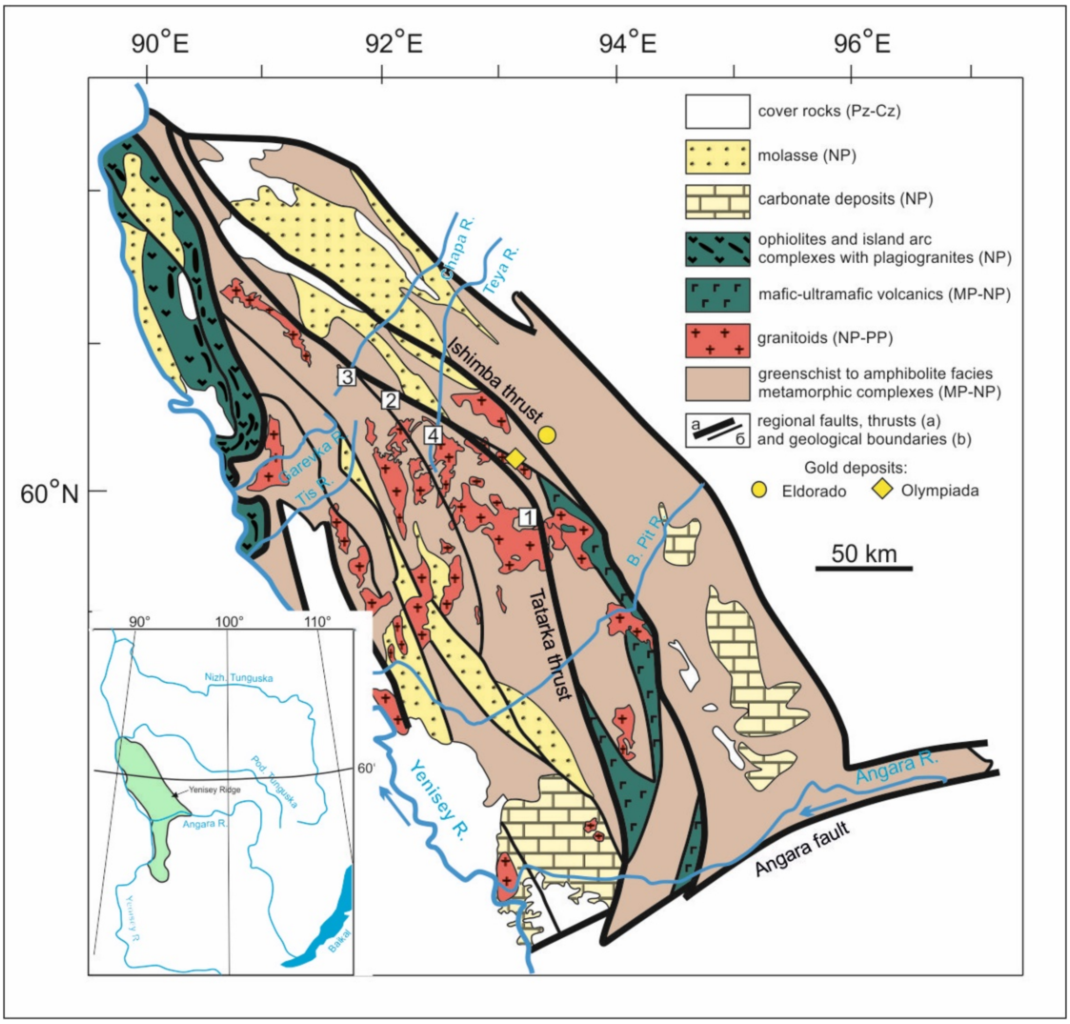

Figure 1. Geological sketch map of the northern part of the Yenisey Ridge showing location of the Olympiada and Eldorado gold deposits and areas mentioned in the text (numbers in squares): 1—Mayakon; 2—Polkan; 3—Chapa, 4—Teya. Compiled after [11,14,24].

3. Geology of Deposits

The Olympiada deposit occurs closer to the Tatarka fault. The deposit is hosted in metamorphosed rocks of the Korda Formation. From top to base, these are carbonaceous quartz-mica schist, foliated marble, quartz-mica-carbonate schist, and biotite-muscovite-quartz schist (Figure 2a). The chemical composition of the rocks ranges from aluminous to carbonate-rich, with minor variations in ferromagnesian content. All rocks are hydrothermally altered to different degrees and contain sulfide mineralization. The principal host rocks are quartz-mica-carbonate (two mica-quartz-calcite) schist and marble. In the underlying quartz-mica (quartz-garnet-mica) and overlying quartz-mica-carbonaceous (carbonaceous silicate) schists, mineralization occurs only near the contacts with carbonate-bearing and carbonate rocks.

Sedimentary rocks are regionally metamorphosed at low amphibolite facies conditions [25,26]. Mineral assemblages are garnet-muscovite-biotite, developed after siltstone. The area of the Olympiada deposit has a local zone of dynamothermal metamorphism and alteration, characterized by distinct mineral assemblages, and spatially restricted to the long-lived tectonic zone along the mineralized horizon. The highest temperature associations of metapelites in the tectonic sliver correspond to the garnet zone (garnet + quartz + biotite ± plagioclase), with sporadic fibrolite-sillimanite and kyanite. Higher pressure rocks correspond to the barrovian type of metamorphism, with mineral assemblages of chloritoid + biotite ± garnet (in metapelite) and margarite + quartz (in metamarl).

The Tyrada and Chirimba massifs of Ayakhta complex (761±8 Ma [27]) are the nearest granitic intrusions to the Olympiada deposit (Figure 2a). The gravity data suggest that all of them are parts of a single batholith [28]. Both massifs are similar in composition, mostly consisting of granodiorite (phase 1) and coarse-grained porphyritic biotite and amphibole-biotite granite of normal alkalinity (main phase 2). These massifs contain numerous internal small stocks, dikes, leucogranite veins, fine-grained granite, and aplite (phase 3).

More than 50 estimates for the age of mineralization exist for the Olympiada deposit based on the K-Ar, $^{40}Ar/^{39}Ar$, Rb-Sr, Sm-Nd, and Re-Os techniques. On the basis of this data a number of main ore-forming stages have been distinguished. The age of the nonauriferous quartz-mica-sulfide mineral association is estimated as 817.1 ± 6.3 to 808.4 ± 7.7 Ma. The age of the main productive quartz-gold-arsenopyrite-pyrrhotite association is 803 ± 6.1 to 758 ± 6.0 Ma, with a prevalence of 795 to 784 Ma. The age estimates of the late quartz-gold-antimony association range from 795.2 ± 5.8 to 660 ± 19 Ma [28].

The Eldorado deposit is much less studied than the Olympiada deposit. It is located near the Ishimba fault (Figure 1). The deposit is situated in the Gorbilok formation of the Sukhoi pit group. The host rocks are garnet-biotite-muscovite schists metamorphosed at low-amphibolite facies conditions. The nearest magmatic rocks are about 15 km away from the deposit and belong to the Kalama granitoid massif of age about 860–880 Ma [13,29]. Twenty-two ore bodies are found in the deposit areas. They form 4 groups (Figure 2b) and are located in subparallel quartz veins with arsenopyrite. Age estimates for this deposit are very restricted. The age of quartz-gold-arsenopyrite stage is estimated as 795 Ma and gold-polysulfide stage as 780 Ma [7]. The age around 790 Ma was obtained by Gibsher et al. [30] for the host metamorphic schists. These were interpreted as the age of the local dynamometamorphism.

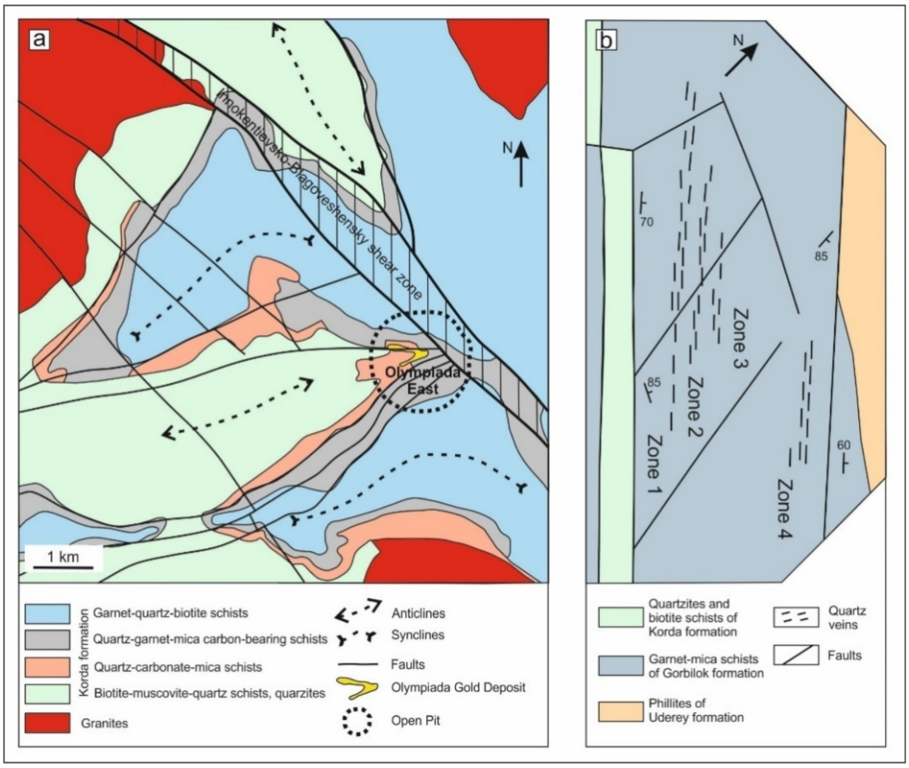

Figure 2. Simplified geological sketch of the (**a**) Olympiada ore field after [28] and (**b**) Eldorado deposit [30].

4. Materials and Methods

Samples of garnet-biotite schists from the Eldorado and garnet-biotite, garnet-staurolite and biotite-muscovite schists from the Olympiada deposits were taken. Samples from the Olympiada deposit were taken from well core which intersects ore bodies. Samples from the Eldorado deposit were taken from the quarry. All schists are enriched in carbonaceous material which forms thin lumpy inclusions in rock-forming minerals: garnet, biotite, muscovite, quartz, chlorite, and chloritoid (Figure 3).

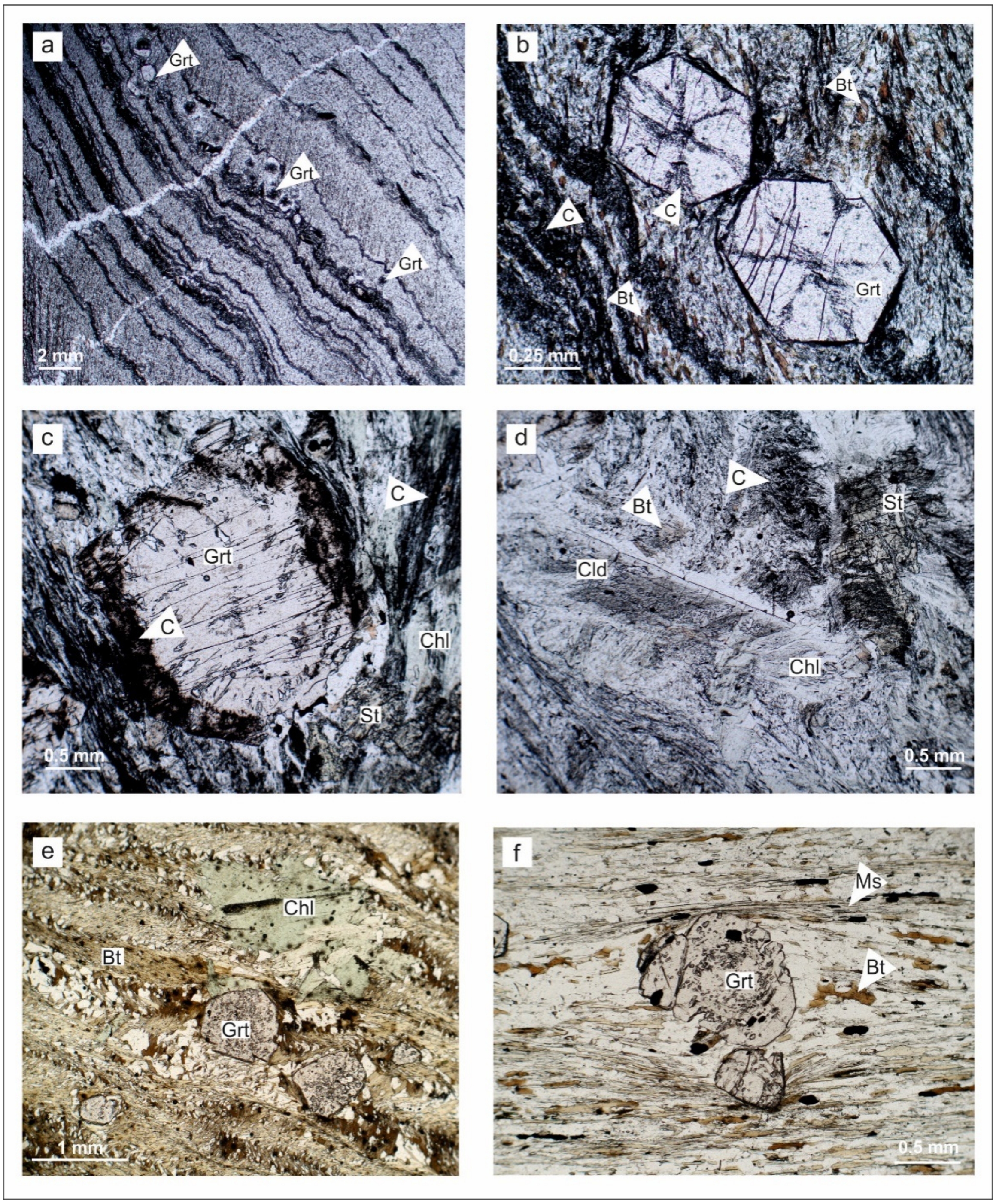

Figure 3. Photomicrograph of thin sections from the host schists of the gold deposits: (**a**–**e**)–Olympiada: (**a**,**b**)—oc-40; (**c**,**d**)—oc-24; (**e**)—oc-99; (**f**)—Eldorado, 19-el-2.

Organic maturity was determined in selected samples on polished sections about 0.2 mm thick, cut perpendicular to the foliation. For the acquisition of the Raman spectra, a Horiba Jobin Yvon LabRam HR confocal Raman spectrometer equipped with a frequency-doubled Nd-YAG laser (100 mW, 532.2 nm) and diffraction gratings of 1200 and 1800 grooves/mm, a Peltier-cooled, slow-scan, ccD matrix-detector and an Olympus bX 40 microscope were used at the Institute of Geology and Mineralogy SB RAS. To obtain a better signal to noise ratio five scans with an acquisition time of 30 sec in the 700–2000 cm^{-1} (first-order) and 2200–3200 cm^{-1} (second-order) region are summed. From 40 to 80 spectra were recorded for each sample. the measured first-order bands of the raman spectra were the D1 [3] or D band [31] at ~1350 cm^{-1}; the G [3] or O band [31] at ca. 1580 cm^{-1}, the D2 band at ~1610 cm^{-1}, and the D3 band at ~1500 cm^{-1}. The second-order bands were recorded at ~2450 cm^{-1}, ~2700 cm^{-1}(s1 band) and ~2900 cm^{-1}(s2 band, [3]). The peak position, area, and peak width (full width at half maximum–FWHM) of the bands were determined using the computer program Fityk 1.3.1. The R1 ratio is calculated as D1/G peak intensity ratio and the R2 ratio is given as D1/(G + D1 + D2) peak area ratio [3].

Minerals for $^{40}Ar/^{39}Ar$ isotopic–geochronologic studies were separated from rocks using conventional techniques of magnetic and density separation. Samples of monomineralic fractions and biotite MCA-11 (OSO no. 129-88, which was used as the mineral monitor) were wrapped in Al foil, placed into a quartz ampoule, which was then pumped out and welded. Biotite MCA-11 (prepared at the Fedorovskii All-Russia Institute of Mineral Resources in 1988 as a K/Ar standard for K/Ar dating) was certified as a $^{40}Ar/^{39}Ar$ monitor with the use of the muscovite Bern 4m and biotite LP-6 internationally certified standards [32]. The integral age of biotite MCA-11 was assumed to correspond to the calibration results: 311.0 ± 1.5 Ma. The quartz ampoules with samples were irradiated in the Cd-coated channel of a reactor (BBP-K type) at the Tomsk Polytechnic Institute. The gradient of the neutron flux did not exceed 0.5% of the sample size. The experiments on the stepwise heating were carried out in a quartz reactor with an external heater. The blank for 40Ar (10 min at 1200 °C) was no higher than 5×10^{-10} ncm^3. Ar was purified using Ti and ZrAl SAES getters. The isotopic composition of Ar was measured on a Noble Gas 5400 (Micromass, United Kingdom) mass spectrometer. The errors quoted below in the text, table, and figures correspond to ±1σ.

5. Results

5.1. Petrography and Mineralogy

Three samples from the well core of Olympiada deposit were taken for detailed study: two samples of garnet-biotite (oc-40 and oc-99) and one of the garnet-staurolite-chloritoid schists (oc-24).

The mineral assemblage of garnet-biotite schists is Grt + Bt + Chl + Pl + Qz. The sample oc-40 has a distinct laminated structure with alternating laminae of a dominantly quartz-feldspar-mica composition containing a small amount of carbonaceous matter and layers enriched with the carbonaceous matter. Garnet is concentrated in certain layers, where it forms idiomorphic porphyroblasts with a sectorial internal structure. The folded structure and the development of schistosity at an angle to the bedding are characteristic of the rock (Figure 3a,b). Garnet composition is xAlm = 0.48–0.63, xPy = 0.03–0.06, xGrs = 0.15–0.17, xSps = 0.34–0.13 (Table 1). The content of almandine, pyrope, and grossular increases to the edges of grains, while the content of spessartine decreases (Figure 4). Biotite contains 1.69–1.82 wt.% of TiO_2 and 0.35–0.37 p.f.u. of Al(VI) (Table 2). Plagioclase has 0.35–0.38 of An component. Chlorite has 25.7–26.3 wt.% of SiO_2 and 21.26–21.44 wt.% of Al_2O_3, xFe (Fe_{total}/Fe_{total} + Mg) = 0.50–0.52 (Table 3).

Table 1. Garnet, muscovite, plagioclase, chloritoid and staurolite composition.

Sample	OC-24						OC-40				OC-99				19-EL-2					19-EL-5				
	Grt r	**Grt c**	**Grt r**	**Ms**	**Cld**	**St**	**Grt 1 r**	**Grt 1 c**	**Grt 1 r**	**Pl**	**Grt r**	**Grt c**	**Grt r**	**Pl**	**Grt r**	**Grt c**	**Grt r**	**Ms**	**Pl**	**Grt r**	**Grt c**	**Grt r**	**Ms**	**Pl**
SiO_2	36.97	37.11	37.23	46.88	24.62	28.43	36.74	37.29	37.38	58.66	37.09	36.67	36.83	62.03	36.97	36.99	37.10	46.61	63.99	36.88	36.63	36.96	46.16	64.44
TiO_2	0.07	0.06	0.02	0.31	0.02	0.42	0.06	0.12	0.06	0.01	0.03	0.14	0.04	0.01	0.02	0.05	0.02	0.28	0.00	0.00	0.06	0.04	0.38	0.00
Al_2O_3	20.89	20.79	21.25	35.43	40.88	54.70	20.63	20.54	20.58	25.79	20.63	20.30	20.50	23.89	20.47	20.54	20.81	35.55	21.59	20.61	20.37	20.22	35.43	21.83
Cr_2O_3	0.00	0.00	0.03	0.03	0.03	0.04	0.04	0.00	0.00	0.01	0.01	0.03	0.02	0.01	0.02	0.00	0.01	0.02	0.00	0.00	0.01	0.03	0.01	0.00
FeO	36.31	34.44	35.77	1.18	25.23	12.48	28.38	21.40	27.71	0.14	34.16	26.58	34.39	0.14	36.68	29.83	35.31	1.08	0.04	35.26	28.90	36.69	1.85	0.07
MnO	0.25	1.98	0.22	0.01	0.03	0.01	6.35	15.12	7.01	0.01	2.48	11.22	1.68	0.00	2.00	9.24	3.45	0.01	0.00	2.91	11.67	2.28	0.00	0.00
MgO	2.36	1.42	1.93	0.60	2.62	0.91	1.39	0.70	1.29	0.00	1.58	1.02	1.63	0.00	1.95	1.32	1.74	0.56	0.00	1.60	1.16	1.92	0.73	0.00
CaO	3.30	4.49	3.34	0.00	0.01	0.01	6.00	5.18	5.90	7.92	4.04	3.25	4.23	5.24	1.96	1.89	2.18	0.00	4.09	2.88	0.91	2.33	0.00	4.10
Na_2O	0.06	0.10	0.06	1.26	0.03	0.01	0.05	0.00	0.00	7.28	0.07	0.10	0.03	8.50	0.02	0.01	0.02	0.92	10.28	0.04	0.01	0.06	1.13	9.49
K_2O	0.02	0.00	0.23	8.67	0.01	0.00	0.00	0.00	0.00	0.08	0.00	0.00	0.00	0.06	0.00	0.00	0.00	10.02	0.05	0.00	0.01	0.00	9.79	0.05
ZnO						0.45																		
	Mole fractions and formula units																							
Si	2.98	3.00	3.00	3.12	2.01	8.20	2.98	3.02	3.02	2.63	3.00	3.01	3.00	2.75	3.01	3.02	3.00	3.10	2.83	3.00	3.01	3.00	3.07	2.85
Ti	0.00	0.00	0.00	0.02	0.00	0.09	0.00	0.01	0.00	0.00	0.00	0.01	0.00	0.00	0.00	0.00	0.00	0.01	0.00	0.00	0.00	0.00	0.02	0.00
Al	1.99	1.98	2.02	2.78	3.94	18.60	1.97	1.96	1.96	1.36	1.97	1.96	1.97	1.25	1.96	1.97	1.98	2.78	1.13	1.97	1.97	1.94	2.78	1.14
Cr	0.00	0.00	0.00	0.00	0.00	0.01	0.00	0.00	0.00	0.00	0.00	0.00	0.00	0.00	0.00	0.00	0.00	0.00	0.00	0.00	0.00	0.00	0.00	0.00
Fe	2.45	2.33	2.41	0.07	1.73	3.01	1.93	1.45	1.87	0.01	2.31	1.82	2.35	0.01	2.49	2.03	2.39	0.06	0.00	2.40	1.98	2.49	0.10	0.00
Mn	0.02	0.14	0.02	0.00	0.00	0.00	0.44	1.04	0.48	0.00	0.17	0.78	0.12	0.00	0.14	0.64	0.24	0.00	0.00	0.20	0.81	0.16	0.00	0.00
Mg	0.28	0.17	0.23	0.06	0.32	0.39	0.17	0.08	0.16	0.00	0.19	0.13	0.20	0.00	0.24	0.16	0.21	0.06	0.00	0.19	0.14	0.23	0.07	0.00
Ca	0.29	0.39	0.29	0.00	0.00	0.00	0.52	0.45	0.51	0.38	0.35	0.29	0.37	0.25	0.17	0.17	0.19	0.00	0.19	0.25	0.08	0.20	0.00	0.19
Na	0.01	0.01	0.01	0.16	0.01	0.01	0.01	0.00	0.00	0.63	0.01	0.02	0.00	0.73	0.00	0.00	0.00	0.12	0.88	0.01	0.00	0.01	0.15	0.81
K	0.00	0.00	0.02	0.74	0.00	0.00	0.00	0.00	0.00	0.00	0.00	0.00	0.00	0.00	0.00	0.00	0.00	0.85	0.00	0.00	0.00	0.00	0.83	0.00
Zn						0.10																		
F	0.90	0.93	0.91		0.84	0.89	0.92	0.95	0.92		0.92	0.94	0.92		0.91	0.93	0.92							
xAlm	0.81	0.77	0.82				0.63	0.48	0.62		0.76	0.60	0.77		0.82	0.68	0.79			0.79	0.66	0.81		
xPrp/xAn	0.09	0.06	0.08				0.06	0.03	0.05	0.37	0.06	0.04	0.07	0.25	0.08	0.05	0.07		0.18	0.06	0.05	0.08		0.19
xGrs/xAb	0.09	0.13	0.10				0.17	0.15	0.17	0.62	0.12	0.09	0.12	0.74	0.06	0.06	0.06		0.82	0.08	0.03	0.07		0.81
xSps/xOrt	0.01	0.04	0.01				0.14	0.34	0.16	0.00	0.06	0.26	0.04	0.00	0.05	0.21	0.08		0.00	0.07	0.27	0.05		0.00

Notes: F = Fe/(Fe + Mg). Formula unita recalculated for Grt-12O, Ms-11O, Pl-8O, St-48O, Cld - 14O.

Table 2. Composition of biotite and Ti-in-Bt temperature.

Sample	OC-24					OC-40					OC-99					19-El-2						19-El-5				
	1	**2**	**3**	**4**	**5**	**1**	**2**	**3**	**4**	**5**	**1**	**2**	**3**	**4**	**5**	**1**	**2**	**3**	**4**	**5**	**6**	**1**	**2**	**3**	**4**	**5**
SiO_2	35.18	35.68	36.07	36.08	36.24	36.54	36.84	36.43	36.75	36.78	36.12	35.91	36.16	36.07	35.62	35.17	35.35	35.46	34.93	35.14	35.99	34.75	35.00	35.69	35.23	34.24
TiO_2	1.62	1.50	1.47	1.41	1.40	1.83	1.75	1.73	1.82	1.78	1.84	1.84	1.84	1.97	1.83	1.68	1.65	1.63	1.68	1.70	1.66	1.68	1.66	1.64	1.59	1.65
Al_2O_3	18.58	18.81	19.16	19.04	18.93	17.49	17.98	18.11	17.74	17.89	18.39	18.34	18.39	18.33	18.26	18.60	18.71	18.83	18.69	18.78	18.88	18.30	18.28	18.48	18.73	18.51
Cr_2O_3	0.00	0.04	0.01	0.01	0.02	0.02	0.05	0.07	0.05	0.05	0.02	0.02	0.03	0.04	0.03	0.09	0.04	0.06	0.05	0.02	0.13	0.02	0.02	0.00	0.01	0.02
FeO	23.82	21.56	21.36	21.21	21.27	20.14	19.74	20.20	19.58	20.29	22.86	23.01	22.69	22.95	23.45	22.13	22.02	21.95	22.55	22.21	22.03	23.63	23.48	22.92	23.15	23.61
MnO	0.01	0.00	0.01	0.01	0.02	0.26	0.28	0.30	0.27	0.28	0.11	0.11	0.10	0.08	0.11	0.03	0.05	0.04	0.03	0.05	0.05	0.04	0.05	0.04	0.03	0.04

Table 2. *Cont.*

Sample	OC-24					OC-40					OC-99					19-El-2						19-El-5				
	1	**2**	**3**	**4**	**5**	**1**	**2**	**3**	**4**	**5**	**1**	**2**	**3**	**4**	**5**	**1**	**2**	**3**	**4**	**5**	**6**	**1**	**2**	**3**	**4**	**5**
MgO	8.41	9.54	9.36	9.49	9.56	9.73	10.07	10.05	10.05	9.82	7.43	7.64	7.54	7.59	7.79	8.15	8.16	8.16	8.22	8.34	8.00	7.11	7.21	7.30	7.46	7.33
CaO	0.00	0.00	0.00	0.00	0.00	0.00	0.00	0.01	0.01	0.00	0.00	0.00	0.00	0.00	0.00	0.00	0.00	0.00	0.00	0.00	0.00	0.00	0.00	0.00	0.00	0.01
Na_2O	0.03	0.25	0.28	0.31	0.26	0.06	0.03	0.08	0.02	0.09	0.06	0.05	0.08	0.06	0.05	0.23	0.18	0.23	0.16	0.21	0.16	0.02	0.14	0.28	0.17	0.00
K_2O	7.63	8.10	8.14	8.16	8.08	9.62	9.60	9.29	9.60	9.42	8.91	8.90	8.96	8.90	8.57	10.39	10.33	10.87	10.27	10.48	10.72	9.65	9.32	9.28	9.32	9.05
Formula Units																										
Si	2.71	2.71	2.73	2.73	2.74	2.78	2.77	2.75	2.78	2.77	2.77	2.75	2.77	2.76	2.74	2.70	2.71	2.70	2.68	2.68	2.72	2.71	2.72	2.75	2.72	2.69
Ti	0.09	0.09	0.08	0.08	0.08	0.10	0.10	0.10	0.10	0.10	0.11	0.11	0.11	0.11	0.11	0.10	0.09	0.09	0.10	0.10	0.09	0.10	0.10	0.09	0.09	0.10
Al	1.68	1.69	1.71	1.70	1.69	1.57	1.60	1.61	1.58	1.59	1.66	1.66	1.66	1.65	1.65	1.68	1.69	1.69	1.69	1.69	1.68	1.68	1.68	1.68	1.70	1.71
Cr	0.00	0.00	0.00	0.00	0.00	0.00	0.00	0.00	0.00	0.00	0.00	0.00	0.00	0.00	0.00	0.01	0.00	0.00	0.00	0.00	0.01	0.00	0.00	0.00	0.00	0.00
Fe	1.53	1.37	1.35	1.34	1.34	1.28	1.24	1.28	1.24	1.28	1.46	1.47	1.45	1.47	1.51	1.42	1.41	1.40	1.45	1.42	1.39	1.54	1.53	1.48	1.49	1.55
Mn	0.00	0.00	0.00	0.00	0.00	0.02	0.02	0.02	0.02	0.02	0.01	0.01	0.01	0.01	0.01	0.00	0.00	0.00	0.00	0.00	0.00	0.00	0.00	0.00	0.00	0.00
Mg	0.96	1.08	1.05	1.07	1.08	1.10	1.13	1.13	1.13	1.10	0.85	0.87	0.86	0.87	0.89	0.93	0.93	0.93	0.94	0.95	0.90	0.83	0.84	0.84	0.86	0.86
Ca	0.00	0.00	0.00	0.00	0.00	0.00	0.00	0.00	0.00	0.00	0.00	0.00	0.00	0.00	0.00	0.00	0.00	0.00	0.00	0.00	0.00	0.00	0.00	0.00	0.00	0.00
Na	0.00	0.04	0.04	0.05	0.04	0.01	0.00	0.01	0.00	0.01	0.01	0.01	0.01	0.01	0.01	0.03	0.03	0.03	0.02	0.03	0.02	0.00	0.02	0.04	0.02	0.00
K	0.75	0.79	0.78	0.79	0.78	0.93	0.92	0.90	0.93	0.91	0.87	0.87	0.88	0.87	0.84	1.02	1.01	1.06	1.00	1.02	1.04	0.96	0.93	0.91	0.92	0.91
F	0.61	0.56	0.56	0.56	0.56	0.54	0.52	0.53	0.52	0.54	0.63	0.63	0.63	0.63	0.63	0.60	0.60	0.60	0.61	0.60	0.61	0.65	0.65	0.64	0.64	0.64
Temperature, °C																										
H2005	549	540	533	524	521	589	580	578	589	581	573	575	574	588	574	559	554	551	558	562	552	554	553	548	542	538
Wu2015	572	546	550	542	539	570	563	560	567	567	614	608	612	619	601	571	569	568	568	569	575	594	591	590	581	570

Notes: Temperature estimates are made using calibrations of Ti-in-Bt thermometers Henry, 2005 (H2005) and Wu, Chen, 2015 (Wu2015). Formula units are recalculated for 22 O.

Table 3. Chlorite compositions and data on chlorite thermometry.

Sample	OC-24							OC-40		OC-99				19-EL-2				
	1	**2**	**3**	**4**	**5**	**6**	**7**	**1**	**2**	**1**	**2**	**3**	**4**	**1**	**2**	**3**	**4**	**5**
SiO_2	24.000	23.960	24.400	24.020	24.120	23.570	23.350	26.345	25.716	24.591	24.983	24.928	24.733	24.570	24.520	24.394	24.673	24.644
TiO_2	0.065	0.048	0.071	0.105	0.056	0.060	0.044	0.057	0.071	0.092	0.071	0.102	0.113	0.081	0.115	0.087	0.053	0.118
Al_2O_3	22.900	22.850	22.700	23.110	23.060	22.430	22.640	21.265	21.441	22.765	22.733	22.942	23.120	23.314	23.420	23.321	23.047	23.104
Cr_2O_3	0.024	0.014	0.000	0.036	0.020	0.024	0.023	0.020	0.054	0.064	0.031	0.063	0.028	0.000	0.031	0.035	0.048	0.000
FeOtotal	29.800	30.160	29.670	29.160	29.820	29.620	29.500	27.481	28.511	30.393	31.199	30.415	30.575	29.476	29.599	29.925	29.515	28.661
MnO	0.024	0.013	0.008	0.017	0.018	0.005	0.022	0.465	0.553	0.173	0.205	0.177	0.177	0.070	0.068	0.067	0.073	0.089
MgO	12.320	12.630	13.140	12.890	12.550	12.610	12.690	15.227	14.463	11.582	11.504	11.198	11.295	12.302	12.330	12.285	12.251	12.495
CaO	0.011	0.000	0.001	0.000	0.022	0.012	0.000	0.028	0.009	0.019	0.000	0.031	0.008	0.015	0.016	0.010	0.043	0.030
Na_2O	0.032	0.000	0.000	0.078	0.029	0.000	0.063	0.049	0.000	0.034	0.000	0.000	0.029	0.025	0.000	0.193	0.204	0.000
K_2O	0.003	0.011	0.002	0.000	0.011	0.003	0.000	0.006	0.038	0.000	0.000	0.011	0.012	0.046	0.000	0.086	0.045	0.032
Total	89.177	89.685	89.991	89.416	89.706	88.334	88.332	90.943	90.856	89.713	90.726	89.867	90.090	89.899	90.099	90.403	89.952	89.173

Table 3. *Cont.*

Sample	OC-24							oc-40		OC-99				19-el-2				
	1	**2**	**3**	**4**	**5**	**6**	**7**	**1**	**2**	**1**	**2**	**3**	**4**	**1**	**2**	**3**	**4**	**5**
Cations Based on 14 oxygen																		
Si	2.541	2.522	2.552	2.525	2.536	2.517	2.489	2.697	2.651	2.603	2.622	2.640	2.611	2.579	2.569	2.545	2.586	2.602
Al(IV)	1.459	1.478	1.448	1.475	1.464	1.483	1.511	1.303	1.349	1.397	1.378	1.360	1.389	1.421	1.431	1.455	1.414	1.398
∑T sites	4.000	4.000	4.000	4.000	4.000	4.000	4.000	4.000	4.000	4.000	4.000	4.000	4.000	4.000	4.000	4.000	4.000	4.000
Al(VI)	1.399	1.356	1.350	1.388	1.393	1.339	1.333	1.263	1.256	1.444	1.435	1.504	1.488	1.463	1.461	1.412	1.432	1.477
Fe(3+)	0.054	0.115	0.088	0.083	0.067	0.133	0.182	0.040	0.083	0.000	0.000	0.000	0.000	0.000	0.000	0.077	0.017	0.000
Fe(2+)	2.584	2.540	2.507	2.480	2.555	2.511	2.448	2.313	2.375	2.691	2.739	2.694	2.699	2.587	2.594	2.533	2.570	2.531
Mn	0.002	0.001	0.001	0.002	0.002	0.000	0.002	0.040	0.048	0.016	0.018	0.016	0.016	0.006	0.006	0.006	0.006	0.008
Mg	1.945	1.982	2.049	2.020	1.967	2.007	2.017	2.324	2.222	1.828	1.800	1.768	1.778	1.925	1.926	1.910	1.914	1.967
Ti	0.005	0.004	0.006	0.008	0.004	0.005	0.003	0.004	0.006	0.007	0.006	0.008	0.009	0.006	0.009	0.007	0.004	0.009
Cr	0.002	0.001	0.000	0.003	0.002	0.002	0.002	0.002	0.004	0.005	0.003	0.005	0.002	0.000	0.003	0.003	0.004	0.000
∑O sites	5.992	5.998	6.000	5.984	5.990	5.998	5.987	5.986	5.994	5.991	6.000	5.995	5.992	5.987	5.998	5.948	5.948	5.992
Oct vacancy	0.008	0.002	0.000	0.016	0.010	0.002	0.013	0.014	0.006	0.009	0.000	0.005	0.008	0.013	0.002	0.052	0.052	0.008
R(2+)	4.531	4.523	4.557	4.502	4.523	4.519	4.466	4.678	4.645	4.534	4.557	4.478	4.493	4.518	4.525	4.449	4.490	4.506
R(3+)	1.461	1.476	1.443	1.483	1.467	1.479	1.521	1.309	1.349	1.457	1.443	1.517	1.499	1.469	1.473	1.499	1.458	1.487
Ca	0.001	0.000	0.000	0.000	0.002	0.001	0.000	0.003	0.001	0.002	0.000	0.004	0.001	0.002	0.002	0.001	0.005	0.003
Na	0.007	0.000	0.000	0.016	0.006	0.000	0.013	0.010	0.000	0.007	0.000	0.000	0.006	0.005	0.000	0.039	0.041	0.000
K	0.000	0.002	0.000	0.000	0.001	0.000	0.000	0.001	0.005	0.000	0.000	0.001	0.002	0.006	0.000	0.011	0.006	0.004
Fe/(Fe*Mg)	0.576	0.573	0.559	0.559	0.571	0.569	0.566	0.503	0.525	0.595	0.603	0.604	0.603	0.573	0.574	0.577	0.575	0.563
Chlorite Crystallisation Temperature																		
ME (°C)	406	411	402	411	408	412	419	356	370	390	384	381	389	397	400	404	393	391
CN (°C)	326	329	323	329	327	330	335	293	302	315	311	310	315	320	322	325	317	316
KM (°C)	369	372	365	371	369	372	377	331	341	359	356	354	359	363	365	368	360	358
J (°C)	413	418	408	417	414	419	426	361	376	397	392	389	397	404	407	411	400	398

Notes: Chemical composition of chlorite and the number of ions in the unit cell calculated based on 14 oxygen with temperature of chlorite crystallization estimated by thermometer of McDowell and Elders, 1980 (ME), Cathelineau and Nieva, 1985 (CN), Kranidiotis and MacLean, 1987 (KM), Jowett, 1991 (J).

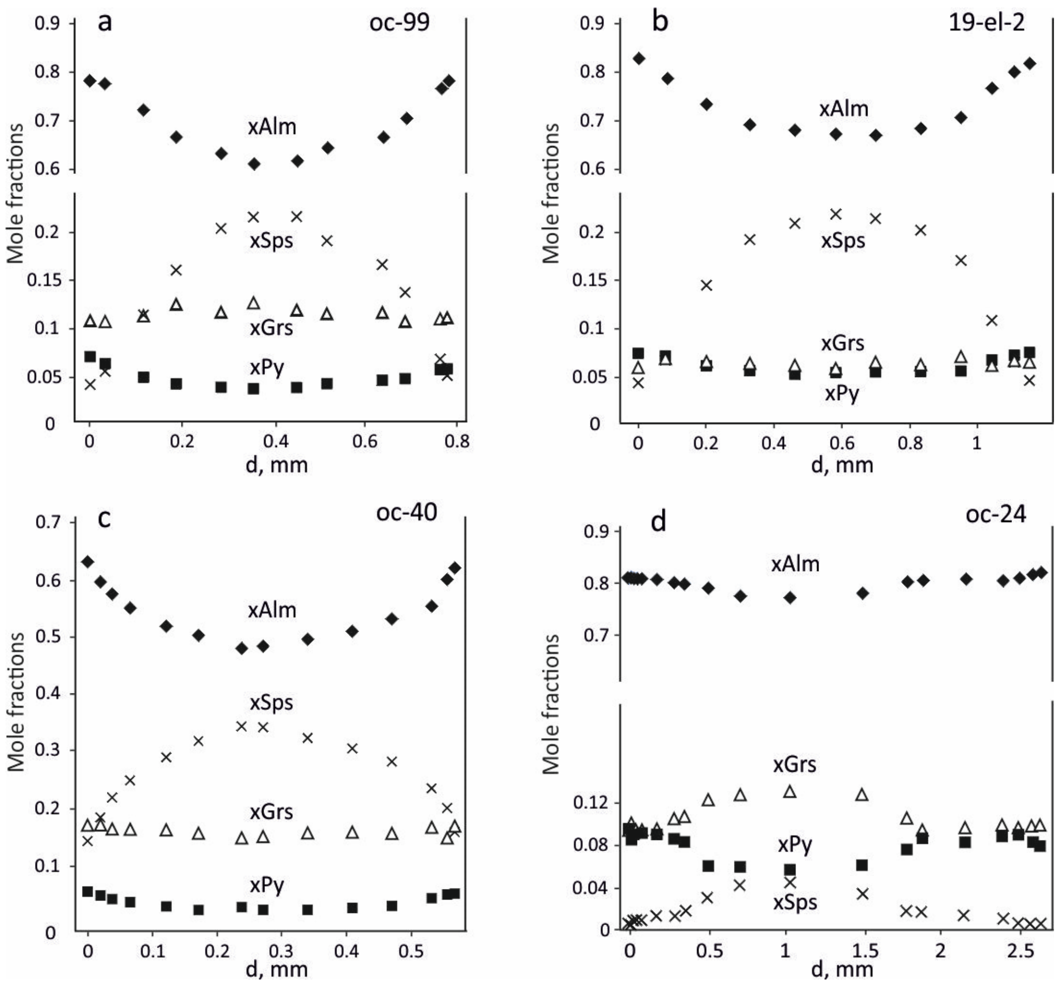

Figure 4. Compositional zoning profiles across garnet crystals of the garnet-biotite (**a**–**c**) and garnet-staurolite-chloritoid (**d**) schists.

Sample oc-99 has a foliated structure (Figure 3e). The rock is composed mainly of biotite (up to 70 vol. %) and garnet (10–15 vol. %), while quartz and plagioclase are less common. The carbonaceous matter is found in insignificant quantities. The composition of the garnet is xAlm = 0.60–0.78, xPrp = 0.04–0.07, xSps = 0.25–0.04, xGrs ~ 0.12 (Table 1). Biotite contains 1.88 wt.% of TiO_2 and xFe (Fe/Fe + Mg) = 0.63 (Table 2). Plagioclase contains xAn = 0.25–0.37 with a decrease in the content of the anorthite component towards the edge parts of the grains. Chlorite contains 24.5–24.9 wt.% SiO_2, 22.7–23.1 Al_2O_3, xFe = 0.59–0.60 (Table 3).

Garnet-staurolite-chloritoid schist (oc-24) has a schistose structure. The rock is significantly enriched in the carbonaceous matter, which occurs in the form of inclusions in garnet, staurolite, chloritoid, chlorite, and micas (Figure 3c,d). In garnet, mainly the edge parts of the grains are enriched with the carbonaceous matter. In staurolite and chloritoid, it is concentrated in the central parts. A sectorial structure is often noted in garnet. Chloritoid, staurolite, and biotite are partially replaced by secondary chlorite. Garnet grains are characterized by a monotonic increase in the almandine component from 0.76 in the central part to 0.82 at the edges and pyrope is from 0.05 to 0.09, respectively (Figure 4, Table 1). At the same time, the spessartine final decreases synchronously (xSps = 0.04–0.01). The content of the grossular component decreases from the core to the edges of the grains (xGrs = 0.13–0.09). The amount of TiO_2 in biotite is 1.4–1.6 wt.% (Table 2). Muscovite is characterized by insignificant contents of celadonite component (Mg + Fe)/(Mg + Fe +

Al(VI) = 0.06 and paragonite component xNa = 0.16. The composition of staurolite from the sample OC-24 is characterized by a high ferrous number (xFe = 0.89) and the presence of minor amount of ZnO = 0.45 wt.%. The ferrous number of the chloritoid is 0.84. Chlorite contains 25–26 wt.% SiO_2, 22.4–23.1 Al_2O_3, xFe = 0.56–0.576 (Table 3).

The host rocks of the Eldorado deposit are rather homogenous in composition. Generally, it is garnet-biotite schist with the mineral assemblage Grt + Bt + Ms + Chl + Pl + Qz. They have lepidoblastic texture with garnet porhyroblasts about 1.2 mm in diameter. Two samples of schists were studied (19-el-2 и19-el-5).

Garnet composition is xAlm = 0.67–0.82, xPy = 0.05–0.07, xGrs = 0.05–0.06, xSps = 0.20–0.04 (Table 1). It has typical prograde zoning with sharply increasing almandine and gently-increasing of pyrope content and decreasing of spessartine content from the core to the rim, grossular varies negligibly (Figure 4). Biotite contains 1.6–1.7 wt.% of TiO_2 and 0.34–0.4 p.f.u. of Al(VI) (Table 2). Plagioclase contains 0.36–0.39 of an component. Chlorite has 24.3–24.6 wt.% of SiO_2 and 23 wt.% of Al_2O_3, xFe (Fe/Fe + Mg) = 0.56–0.57 (Table 3).

5.2. P-T Parameters of Metamorphism

Temperature estimates have been made with a garnet-biotite geothermometer [33] and a Ti-in-Bt geothermometer [34,35], pressure has been estimated with a garnet-biotite-plagioclase geobarometer [36]. For P-T calculations composition of garnet and plagioclase rims and biotite from the rocks matrix were taken. These minerals do not form reaction textures with each other and do not indicate other evidence of disequilibrium.

Olympiada. Temperature estimates for garnet-staurolite-chloritoid schists (sample oc-24) were performed using 60 garnet-biotite couples. Obtained results fall into the range from 555 to 580 °C, average meaning 565 °C, standard deviation (sd) = 6.7. Ti-in-Bt temperature estimates vary from 530 to 550 °C (Table 2).

Garnet-biotite schists. For the sample oc-40 sixty garnet-biotite couples were taken for temperature estimates. Obtained parameters fall into the range 515–545 °C, average 530 °C, sd = 7.2. Ti-in-Bt thermometry indicates temperature range 560–580 °C. For the sample oc-99: temperature interval 555–590 °C, average (from 60 couples) 570 °C, sd = 8.0, Ti-in-Bt temperature—570–610 °C (Table 2).

Pressure estimates for garnet-biotite schists 6.0–7.0 (average 6.5) kbar and 6.8–7.8 (average 7.3) kbar for the samples oc-40 and oc-99 correspondingly.

Ten other samples of garnet-biotite schists were taken from the same well core. They have mineral composition and compositions of rock-forming minerals similar to those for schists described above. We do not show here its detailed description, obtained P-T parameters fall into the range: Grt-Bt [33]—540–570 °C, Ti-in-Bt [34]—560–590 °C, pressure 6.3–7.4 kbar (Table 4).

Table 4. P-T parameters of metamorphism of garnet-biotite schists of the Olympiada deposit.

Sample	T, °C		P, kbar
	Ti-in-Bt	Grt-Bt	Grt-Bt-Pl-Qtz
OC107	577	540	6.3
OC05	560	580	6.5
OC06	570	545	6.7
OC95	590	555	7.4
OC99	595	550	6.9
OC100	565	565	6.6
OC102	585	575	6.8
OC119	560	570	7.2
OC120	580	550	6.5
OC49	590	565	7.4

Eldorado. Temperature estimates on the basis of the Grt-Bt geothermometry fall into the following intervals. For the sample 19-el-2: 550–575 °C, average 560 °C, sd = 5.5 (from

48 couples). Ti-in-Bt thermometry [34] indicates temperature 550–570 °C, for the sample 19-el-5: 564–588 °C, average 576 °C, sd = 5.9 (from 48 couples). Average pressure estimates for both samples are 6.1–6.5 kbar.

5.3. Chlorite Thermometry

Mineral microtextures indicate that chlorite in samples from the Olympiada deposit replaces minerals of the peak metamorphic assemblage: biotite, staurolite, and chloritoid (Figure 3). For the temperature estimates, chlorite thermometry has been applied. Both empirical and semi-empirical approaches were used for chlorite geothermometry, and results obtained are summarized in Table 3. Among the empirical methods, four different geothermometers of Kranidiotis and MacLean [37] (KM), Jowett [38] (J), McDowell and Elders, [39] (ME) and Cathelineau and Nieva [40] (CN) were used. The highest temperature (390–410 °C) was indicated by thermometers of Jowett [38] and McDowell and Elders [39] for samples oc-24, oc-99 and 19-el-2 and slightly less (350–370 °C) for the sample oc-40. Calibrations CN and KM indicate lower temperature in the range 310–370 °C.

The semi-empirical approach of Bourdelle et al. [41] was also used as it is best suited for low temperature chlorites (<350 °C). Individual T-R^{2+}-Si diagrams (where T—temperature, R^{2+}—sum of divalent cations, Si [apfu]) were plotted and temperatures were graphically estimated (Figure 5). Most of the chlorites in T-R^{2+}-Si diagram plot above 350 °C isotherm. Since, the optimal reliability of this thermometer is up to 350 °C only, this method could not estimate the upper temperature limit of chlorites but it clearly indicates that for all chlorite the upper temperature limit is higher than 350 °C.

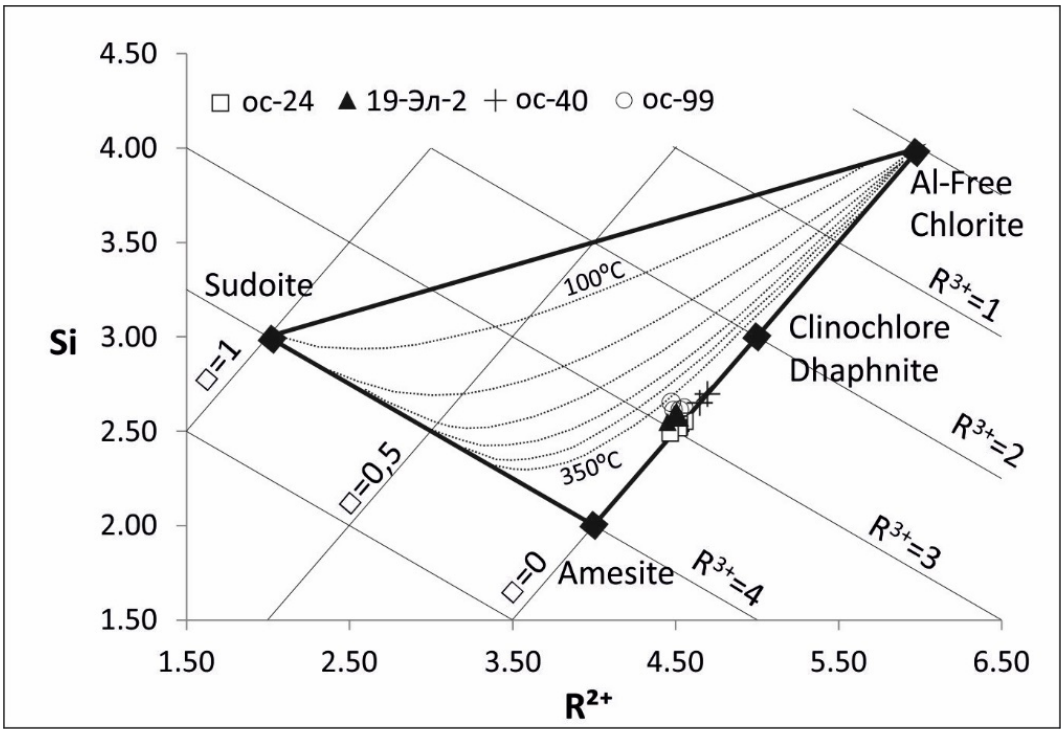

Figure 5. Representation of compositional data set of chlorite in the R^{2+}-Si diagram of Wiewiora and Weiss [42]. Isotherms (in 50 °C steps) calculated with Bourdelle et al. [41] geothermometer.

5.4. Raman Spectroscopy

Carbonaceous matter (CM) inclusions in garnet, quartz, chloritoid and micas (Figure 6) were analyzed. From 44 to 79 measurements were made for each sample (Table 5). CM particles were analyzed in situ enclosed within transparent grains in sections orientated perpendicular to the foliation. Raman spectra acquired from samples display sharp and intense G peaks at ~1578 cm^{-1}, D1 peaks at ~1347 cm^{-1}, and weakly resolved, broad shoulders of the D1 bands at ~1615 cm^{-1} indicating the D2 peak (Figure 7). The second-order spectra are characterized by bands at ~ 2693 cm^{-1}(Table 5). D1 bands at ~1353 cm^{-1} and G peaks at ca. 1576 cm^{-1}were measured on the first-order Raman spectra of samples.

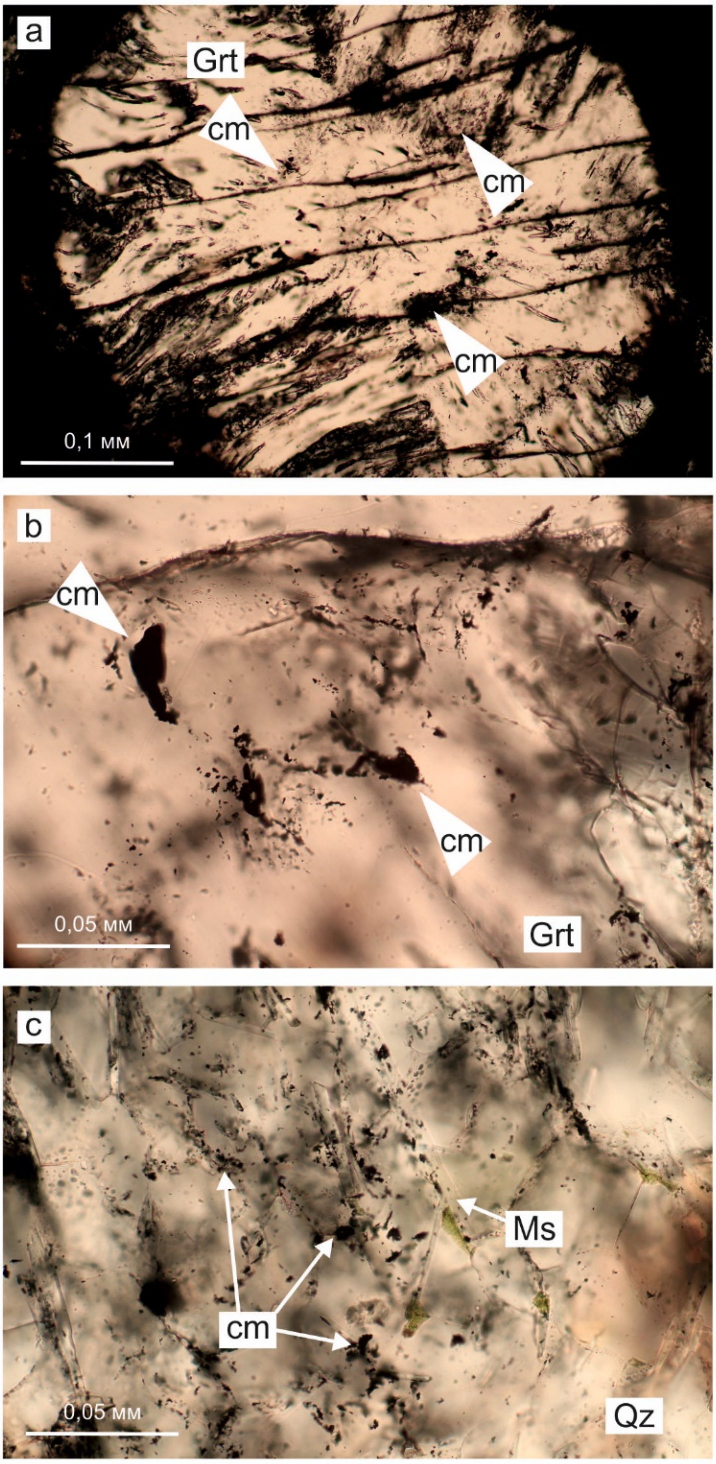

Figure 6. Photomicrograph of carbonaceous material (cm) in garnet (**a**,**b**) and muscovite (**c**) from the sample oc-24.

Table 5. Raman spectra position, FWHM and estimated temperature.

Sample	n	D1				G				D2				R1		R2		Temperature (°C)					
		Position		FWHM		Position		FWHM		Position		FWHM						Beyssac et al. [2]			Rahl et al. [43]		
		Mean	SE	Mean	SE	Mean	Se	Mean	Se	Mean	Se	Mean	Se	Mean	Se	Mean	Se	Mean	Min	Max	Mean	Min	Max
oc-24	78	1350.0	3.7	46.4	1.4	1576.0	2.3	20.0	1.3	1616.5	2.7	14.8	3.7	0.3	0.1	0.3	0.1	508	413	579	495	374	617
oc-40	44	1353.4	2.4	45.1	1.4	1576.5	1.4	21.1	2.5	1617.2	1.9	11.8	2.6	0.3	0.1	0.3	0.0	511	470	562	504	437	588
oc-99	79	1353.8	2.7	44.1	1.5	1577.7	1.4	19.7	1.8	1618.9	1.9	11.0	2.2	0.2	0.1	0.2	0.1	539	461	612	548	428	681
19-El-2	67	1355.2	3.1	44.2	2.7	1577.0	2.0	17.6	1.0	1600.0	34.2	12.6	3.7	0.2	0.1	0.2	0.1	546	451	607	558	400	670
19-El-5	63	1352.2	4.3	44.2	2.8	1574.8	3.4	18.5	1.8	1615.0	4.1	14.2	3.3	0.1	0.1	0.2	0.1	561	496	611	586	477	678

Notes: R1 and R2 reported here are averages Raman spectra collected per sample. Uncertainties are represented by standard errors (SE), which were determined by dividing the standard deviation of the measurements by the square root of the number of measurements.

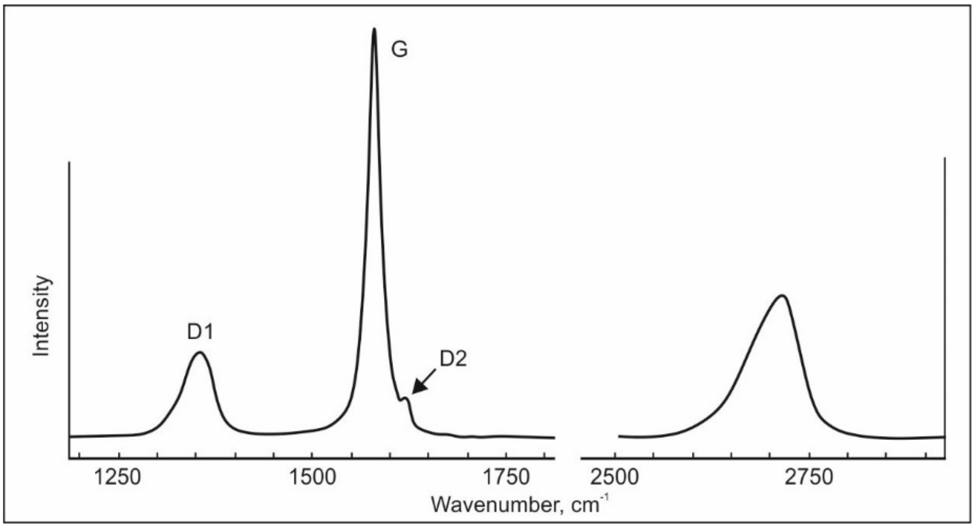

Figure 7. An example Raman spectrum of CM from the sample oc-24 from Olympiada deposit, illustrating four distinct peaks.

In the geothermometer of Beyssac et al. [4] metamorphic temperature is calculated as a linear function of the R2 parameter (R2 = D1/(G + D1 + D2) area ratio) and the thermometer is calibrated in the range of 330–650 °C. The calibration of geothermometerby Rahl et al. [43] is based on both R1 (R1 = D1/G high ratio) and R2 parameters and is applicable for temperatures as low as 100 °C. Both of these calibrations were used for temperature estimates and they indicated very similar results (Table 5). Temperatures obtained for each sample fall into a wide range around 100–150°C around the mean temperature (Table 5, Figure 8). CM inclusions in different minerals (garnet, quartz, muscovite, and chlorite) indicate a large scatter of crystallinity in each mineral phase (Figures S1 and S2).

5.5. Ar-Ar Dating

More than 50 estimates for the age of mineralization exist for the Olympiada deposit based on various techniques, whereas the age data on the Eldorado deposit is very restricted.

Gold at the Eldorado deposit mostly resides in quartz rather than in sulfides and is of two generations, associated with carbon-saturated quartz and early sulfides (arsenopyrite and pyrite) or with late complex ore mineralization (sphalerite, chalcopyrite, and galena). Gold of the first generation is invisible, with small particles more strongly deformed and uniformly distributed, which makes up the greatest part of the gold reserves, while the particles of the second generation gold are coarser.

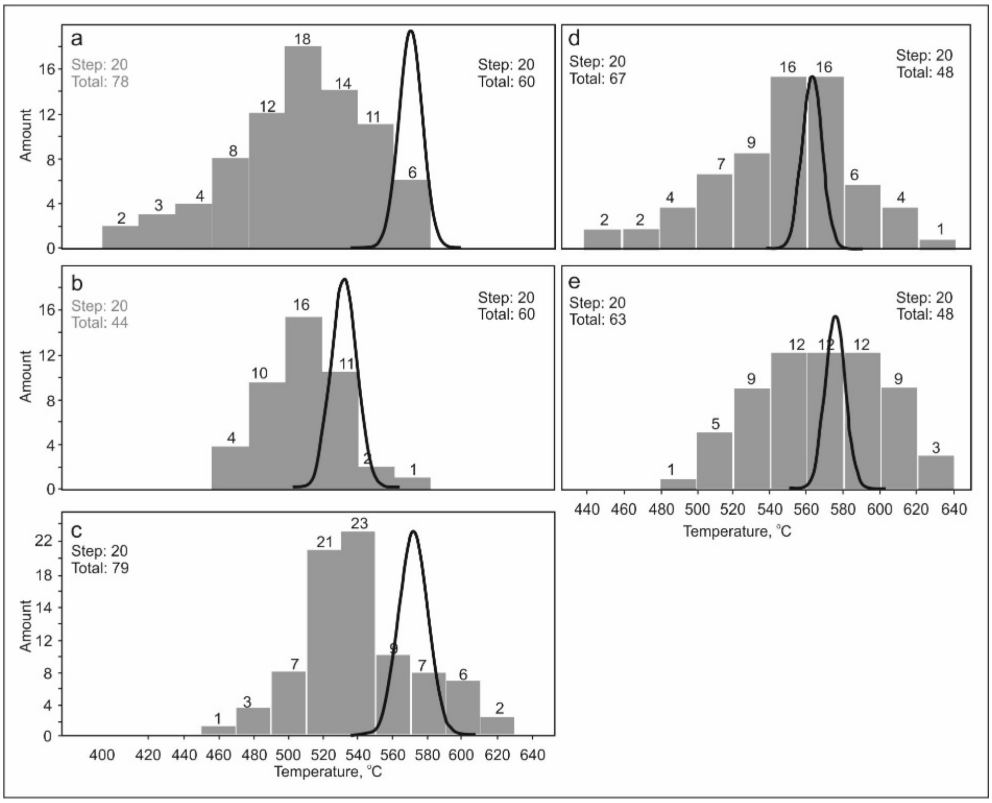

Figure 8. Distribution histograms of temperatures estimated with carbonaceous material thermometry [3]. Black peaks show distribution of temperatures obtained with Grt-Bt thermometry for the same samples (uncertainty of geothemometer is not considered). (**a**–**c**)—Olympiada deposit: (**a**)—oc-24, (**b**)—oc-40, (**c**)—oc-99; (**d**,**e**)—Eldorado: (**d**)—19-el-2, (**e**)—19-el-5.

$^{40}Ar/^{39}Ar$ dating was performed for clarification of ore processes of the Eldorado deposit. For dating a sample of quartz vein with fragments of host garnet-biotite schists was taken. Quartz veins in garnet-biotite schists do not cross schistosity of host rocks and contain its lens-shaped fragments, mean while they are deformed conformal to host schists and often form lenses in it (Figure 9a). No retrograde changes like secondary chlorite were noticed (Figure 9b). Quartz contains inclusions of large arsenopyrite crystals (up to 1 cm) and is cut by a light-green sericite vein, which contains arsenopyrite grains as well (Figure 9c). The concentration of gold in the sample is about 5.3 ppm. For dating of the younger age limit of the ore mineralization, the fine-grained sericite was taken. Obtained plateau includes 58.4% of the total argon and indicates the age 798.6 ± 5.3 Ma (Figure 9d, Table 6).

Table 6. Ar-Ar sericite data.

Heating Step	T (°C)	^{40}Ar/^{39}Ar	±1σ	^{38}Ar/^{39}Ar	±1σ	^{37}Ar/^{39}Ar	±1σ	^{36}Ar/^{39}Ar	±1σ	Ca/K	$\sum^{39}$Ar (%)	Age, Ma	±1σ
Sample Eld-642 (sericite), Weight = 8.8 mg, J = 0.003175 ± 0.000026													
1	500	71.3	0.141	0.086	0.00216	1103.652	70.38	0.0974	0.00395	3973.1	2.4	228.7	6.2
2	600	116.7	0.18	0.06	0.00135	716.613	39.93	0.0531	0.00164	2579.8	6.4	502	4.2
3	700	150.7	0.255	0.049	0.00082	521.11	16.63	0.0592	0.00142	1876	13.5	636.4	4.8
4	750	177.5	0.129	0.023	0.00068	158.15	16.39	0.0074	0.00109	569.34	27.8	798.3	5.4
5	800	180.6	0.103	0.023	0.00054	65.813	12.22	0.0121	0.00077	236.93	45.8	804.4	5.4
6	900	180.3	0.124	0.028	0.00049	220.31	17.23	0.0193	0.00059	793.12	60.7	795.8	5.3
7	1000	180.7	0.171	0.028	0.00067	134.609	24.06	0.0207	0.00153	484.6	71.9	795.6	5.6
8	1130	191.1	0.087	0.024	0.00035	71.454	8.19	0.0248	0.00054	257.2	100	829.3	5.5

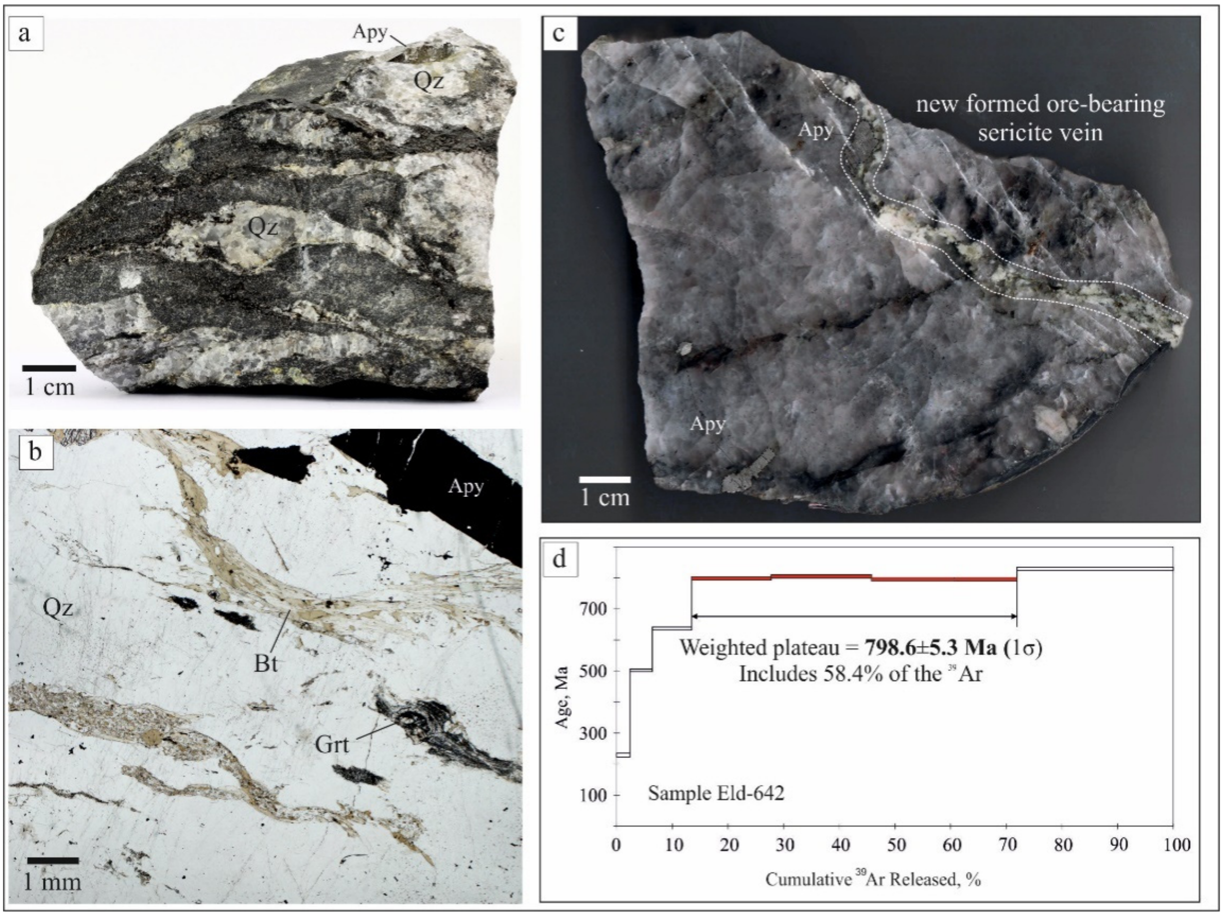

Figure 9. Photograph of the sample of quartz vein in garnet-biotite schist from the Eldorado deposit (**a**), photomicrograph of thin section of quartz vein with relicts of host schists and inclusions of arsenopyrite (**b**), quartz vein cut by sericite vein used for Ar-Ar dating (**c**), weighted plateau of Ar-Ar age of sericite (**d**).

6. Discussion

6.1. P-T Conditions of Metamorphism

Conventional thermometry data indicate that the metamorphism of garnet-biotite and garnet-staurolite schists occurred at temperatures of about 530–570 °C and pressure mainly around 6–7 kbars and they were very similar for both deposits. Similar P-T parameters were obtained in earlier works (see review of Sazonov et al. [2]) and they correspond to the P-T parameters of Barrovian metamorphism estimated in the Mayakon area [20] (Figure 10).

Late chlorite is typical for schists from the Olympiada deposit; relatively high temperatures obtained by chlorite thermometry (more than 350 °C) indicate that chlorite was formed probably due to low-temperature metamorphism, but not in a hydrothermal environment.

Typical prograde metamorphic zoning in garnets with decreasing spessartine and increasing almandine from core to the rims and almost homogenous in grossular content indicates a single stage of prograde metamorphism. The rocks do not have any evidence of early HT/LP metamorphism which was mentioned in the nearest area [20] or the grade of early metamorphism was not higher than greenschist facies. This shows that the early stage of metamorphism described over the whole YR [44] probably has a patchy distribution.

Detailed studying of metamorphic processes of Transangarian part of YK was performed along Tatarka thrust (Figure 1, review [44] and references therein). Fe- and Al-rich metapelitic schists of the Korda formation show petrological evidence of two superimposed metamorphic events. An early middle Proterozoic event produced low-pressure, andalusite-bearing assemblages at c. 3.5–4 kbar and 540–560 °C. During a subsequent late Proterozoic event, a moderate-pressure (Barrovian-type), regional metamorphic overprint produced kyanite-bearing mineral assemblages that replaced minerals formed in the low-pressure event [21]. Due to these two metamorphic events, a specific chemical zoning with sharp increasing of grossular component from core to the rims develops in garnet grains [20,21].

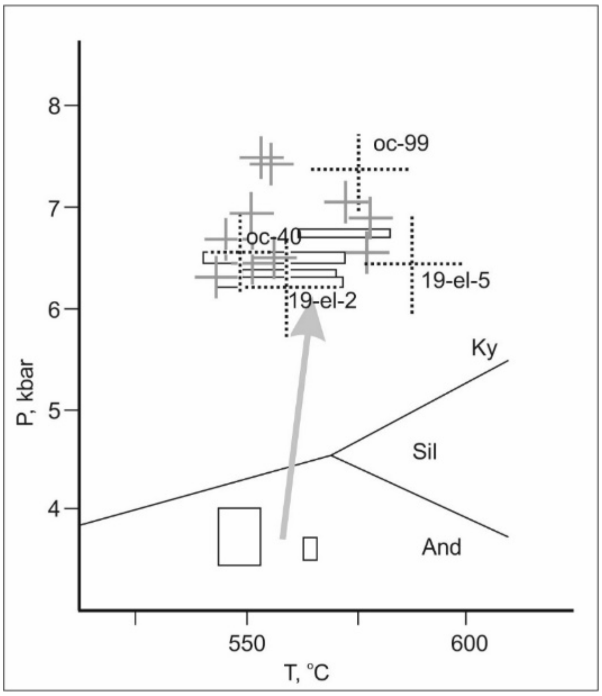

Figure 10. Pressure-Temperature diagram with parameters of metamorphism of the Mayakon area (rectangulars) [20] and Olympiada and Eldorado schists (crosses). Grey arrow shows the PT-path of schists of the Mayakon area from early HT/LP metamorphism to the late Barrovian-type metamorphism [20].

The early stage considered to be occurred as a result of the orogeny during late Meso-early Neoproterozoic. This is supported by earlier U–Th–Pb, Rb–Sr, and K–Ar data on granite-gneiss domes (1100–950 Ma) and the more recent single-zircon (U–Pb SHRIMP II) and 40/39Ar dating of metapelites, metabasites, and rapakivi granites (1140–870 Ma) [13,22,45]. The age estimates around c. 1050 Ma, were obtained by U-Th-Pb dating of xenotime inclusions in the core of zoned garnet grains [21]. The age of the second (Barrovian-type) metamorphic episode is estimated in the range from 850 to 800 Ma. Age estimates are based on CHIME monazite dating [21] and much Ar-Ar data on biotite from metamorphic schists around the whole YK [13,20–22,30].

This review indicates the strong correlation of Barrovian-type metamorphism with the time interval 800–850 Ma in the YK collisional orogen. Mineral assemblages and compositional zoning in garnets from both Eldorado and Olympiada deposits indicate that the rocks underwent only one episode of metamorphism with PT-parameters the thermal gradient of Barrovian type of metamorphism and do not have evidence of the early stage. In the light of regional studies we can suggest that the age around 840 Ma obtained for host schists of Eldorado deposit should be considered as an age of a single metamorphic event, but not a local dynamometamorphism as was suggested by Gibsher et al. [30] and that there is no evidence of early metamorphism with the age around 1050.

6.2. Carbonaceous Material Thermometry

Previous studies [46] have shown that a large range of crystallinity is characteristic of carbonaceous matter of organic origin, in contrast to that precipitated from the fluid phase. The temperature obtained on the basis of CM Raman spectra falls in a wide range of about 100–150 °C around the mean temperature for each sample, which suggests varying degrees of graphitization for CM particles in the sample. A large scatter of CM crystallinity inside a single mineral phase indicates that it does not depend on the structural position in the rock. This range exceeds the dispersion of the points for the calibration of the CM thermometer ±50 °C suggested by Beyssac et al. [3]. As no different morphological types of CM were found in samples, this heterogeneity may be due to heterogeneity of the carbonaceous matter or different orientation of microdomains inside a single CM particle. The influence of the mineral matrix or composition of the metamorphic fluids is not excluded [47].

Comparison of data obtained by conventional and CM thermometry shows that the Grt-Bt temperature estimates are generally close to the highest temperatures obtained by CM thermometry (Figure 8) and most CM temperature estimates are much lower than data of Grt-Bt thermometry. This is most pronounced for samples from the Olympiada deposit (Figure 8a–c).

These data indicate that thermometry using Raman spectroscopy of carbonaceous material is a reliable tool for temperature estimates in the temperature range 500–600 °C, but it can only be used if there is a sufficiently large number of analyzes.

6.3. Ar-Ar Dating

The sericite vein that was used for Ar-Ar dating cuts the host gray quartz vein and trapped fragments of biotite schist. Arsenopyrite grains are located in both quartz and sericite veins (Figure 9), which implies sericite growth simultaneously or later than arsenopyrite. This is consistent with the Ar-Ar date of 798.6 ± 5.3 Ma as an age of quartz-gold-arsenopyrite mineralization or its younger age limit. These data are similar to the age of quartz-gold-arsenopyrite stage (795 Ma) and gold-polysulfide stage (780 Ma) obtained earlier by Sazonov et al. [7].

6.4. Correlation of the Mineralization Periods with the Main Tectonomagmatic Events

Correlation of the mineralization periods with the main tectonomagmatic events [13,14,22,27,28,30] in the region shows the following. In the early Neoproterozoic (1050–950 Ma), the terrigenous strata of the Sukhoi Pit Group were deformed and metamorphosed as a result of orogeny. These processes were most intense in the Tatarka–Ishimba fault system. In the earlier, syncollisional, period of this stage, the formation of Teya-type granite-gneiss domes was accompanied by extensive pegmatization [13]. The late collisional period (880–860 Ma) was marked by the formation of K–Na granitoid plutons of the Kalama type (Teya-Eruda complex) [13,27]. Premineral metasomatites formed in a large contact aureole, in the zone where these plutons influenced enclosing black shale–terrigenous strata. They host Au fields and deposits, which formed later.

Barrovian-type metamorphism took place at ~860–800 Ma [21,23]. It is genetically related to thrusting and the final stage in the evolution of a collisional orogen. Two following stages of metamorphism were distinguished [23]. The early stage of collisional metamorphism with the peak around 860–850 Ma was related to mostly westward thrusts of blocks of Siberian craton, the late collisional stage around 800 Ma—with eastward thrusts of the Central Angara terrane to the Siberian craton [21].

The formation of quartz-vein zones (Sovetskoe, Eldorado, and other deposits) (830–820 Ma) correlates well with that of thrust nappes. The paragenetic relationship between quartz veining and thrust nappes is confirmed by the fact that quite complex synfolding veins have obvious features of metamorphic bodies [48,49]. The late collisional metamorphism (802–798 Ma) caused by eastward movements of blocks in the zone of high order splays developed at this stage [23]. The formation of bimodal dike swarm dated at ~790 Ma is related to Neoproterozoic extension along the western margin of Siberian Craton and mark the upper age limit of collisional metamorphism

In the Late Neoproterozoic, rift and intraplate magmatism was most intense and frequent in the Tatarka–Ishimba fault system. Here, we distinguish four stages in the formation of rift structures, accompanied by intraplate magmatism at 780, 750, 700, and 670–650 Ma. The formation of gold–sulfide ores (720–711 Ma) parallels the initiation and evolution of rift structures (Uvolga, Indola, Talovka grabens, Teya–Chapa trough) (720–700 Ma) as well as intraplate subalkaline granitoid and alkaline magmatism (Kutukas and Gurakhta granitoid complexes, 690–700 Ma; Zakhrebetnaya and Middle Tatarka complexes, 700–710 Ma). The time of Au–Sb mineralization correlates with the pre-Vendian orogeny, the initiation of fault grabens infilled with the Chapa Group sediments, and the emplacement of alkalic–ultramafic intrusions (670–650 Ma). The latest postmineral alterations of mineral matter may be related to the tectonomagmatic processes manifested in syenite–alkali syenite (Middle Vorogovka complex) and subalkalic granitoid (Tatarka massif) intrusions with an age of 630–620 Ma.

This review indicates that the most productive quartz-gold-arsenopyrite stage correlates well in time with the collisional stage (800–850 Ma) and formation of barrovian-type metamorphic complexes over the whole YK (Figure 11), where as the closest magmatic events occurred much earlier (Teya-Eruda complex) or much later (Ayahta complex). This implies that metamorphic processes can play a key role in forming YK gold deposits.

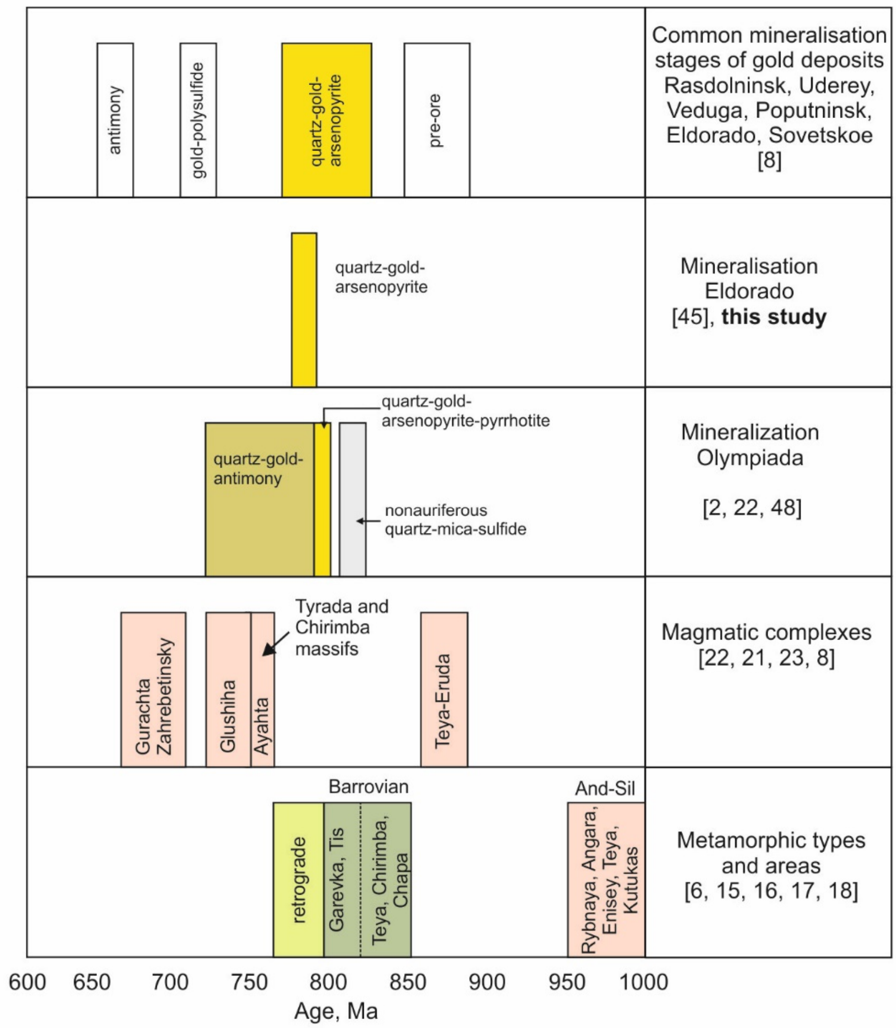

Figure 11. The time correlation scheme of main magmatic and metamorphic events with mineralization stages of gold deposits of the Yenisey Ridge.

7. Conclusions

(1) The host rocks of both Olympiada and Eldorado gold deposits are metamorphosed during the single episode of Barrovian-type metamorphism at similar temperatures 530–570 °C. The rocks do not indicate any traces of the early HT/LP metamorphism observed in other areas of the YK. The growth of the late chlorite after peak metamorphic minerals occurred at temperatures higher than 350 °C probably during retrograde metamorphism.

(2) Carbonaceous material thermometry indicates a wide range of obtained temperatures around 90–150 °C for each sample. The highest temperatures are close to the peak metamorphic temperatures estimated by garnet-biotite thermometry. We guess that thermometry using Raman spectroscopy of carbonaceous material is a reliable tool for temperature estimates, but it can only be used if there is a sufficiently large number of analyzes.

(3) The new 39/40Ar age data on ore-forming processes of the Eldorado deposit around 796 Ma are very close to the age of the Barrovian-type metamorphism estimated in the area under study and around the whole Yenisey ridge. This may indicate their genetic affinity.

(4) The review of magmatic and metamorphic events and ore-forming processes of Yenisey ridge indicate that the most productive ore stage (gold-sulfide-quartz) have a good time correlation with the regional metamorphism of Barrovian type. This indicates that metamorphic processes can play a key role in forming of gold deposits of the Yenisey ridge.

Supplementary Materials: The following are available online at https://www.mdpi.com/article/10.3390/geosciences11110452/s1, Figure S1: Distribution histograms of temperatures estimated with carbonaceous material thermometry [3] for different mineral phases. a-OC-24, b-OC-40, c-OC-99; Figure S2: Distribution histograms of temperatures estimated with carbonaceous material thermometry [3] for different mineral phases. a-19-El-5, b-19-El-2.

Author Contributions: Conceptualization and methodology, V.S.; software, V.V.; formal analysis, V.S., V.V. and P.K.; investigation, V.S. and V.V.; resources, V.S. and P.N.; writing—original draft preparation, V.S.; writing—review and editing, V.S.; visualization, V.S., V.V. and P.N.; supervision, V.S.; project administration, V.S.; funding acquisition, V.S. All authors have read and agreed to the published version of the manuscript.

Funding: The fieldwork and Ar/Ar dating were done on the state assignment of IGM SB RAS and IGG UB RAS with the financial support of the Ministry of Science and Higher Education of the Russian Federation. The studying of metamorphic conditions and Raman spectroscopy of carbonaceous material were done with the financial support of the Russian Science Foundation (RSF), grant No. 21-77-20018 (Metamorphic complexes of the Yenisey Ridge: geological evolution, sedimentary parent rocks, and resource potential).

Conflicts of Interest: The authors declare no conflict of interest.

References

1. Large, R.R.; Bull, S.W.; Maslennikov, V.V. A Carbonaceous Sedimentary Source-Rock Model for Carlin-Type and Orogenic Gold Deposits. *Econ. Geol.* **2011**, *106*, 331–358. [CrossRef]
2. Sazonov, A.M.; Lobanov, K.V.; Zvyagina, E.A.; Leontiev, S.I.; Silyanov, S.A.; Nekrasova, N.A.; Nekrasov, A.Y.; Borodushkin, A.B.; Poperekov, V.A.; Zhuravlev, V.V.; et al. Olympiada Gold Deposit, Yenisei Ridge, Russia. *SEG Spec. Publ.* **2020**, *23*, 203–226.
3. Beyssac, O.; Goffe´, B.; Chopin, C.; Rouzaud, J.N. Raman spectra of carbonaceous material in metasediments: A new geothermometer. *J. Metamorph. Geol.* **2002**, *20*, 859–871. [CrossRef]
4. Beyssac, O.; Bollinger, L.; Avouac, J.-P.; Goffe´, B. Thermal metamorphism in the lesser Himalaya of Nepal determined from Raman spectroscopy of carbonaceous material. *Earth Planet. Sci. Lett.* **2004**, *225*, 233–241. [CrossRef]
5. Rantitsch, G.; Grogger, W.; Teichert, C.; Ebner, F.; Hofer, C.; Maurer, E.-M.; Schaffer, B.; Toth, M. Conversion of carbonaceous material to graphite within the Greywacke Zone of the Eastern Alps. *Acta Diabetol.* **2004**, *93*, 959–973. [CrossRef]
6. Grew, E.S. Carbonaceous Material in Some Metamorphic Rocks of New England and Other Areas. *J. Geol.* **1974**, *82*, 50–73. [CrossRef]

7. Pasteris, J.D.; Wopenka, B. Raman spectra of graphite as indicators of degree of metamorphism. *Can. Mineral.* **1991**, *29*, 1–9.
8. Bibikova, E.V.; Gracheva, T.V.; Makarov, V.A.; Nozhkin, A.D. Age boundaries in geological evolution of the Early Precambrian of the Yenisey Ridge. *Stratigr. Geol. Correl.* **1993**, *1*, 35–40. (In Russian)
9. Sukhorukov, V.; Turkina, O.; Tessalina, S.; Talavera, C. Sapphirine-bearing Fe-rich granulites in the SW Siberian craton (Angara-Kan block): Implications for Paleoproterozoic ultrahigh-temperature metamorphism. *Gondwana Res.* **2018**, *57*, 26–47. [CrossRef]
10. Sukhorukov, V.; Turkina, O.; Tessalina, S.; Talavera, C. Orthopyroxene-sillimanitegranulites of the Angara-Kan block (SW Siberian craton): Constraints on timing of UHT metamorphism. *J. Asian Earth Sci.* **2021**, *207*, 104650. [CrossRef]
11. Likhanov, I.I.; Nozhkin, A.D.; Reverdatto, V.V.; Kozlov, P.S. Grenvillian tectonic events and evolution of the Yenisei Ridge at the western margin of the Siberian craton. *Geotektonics* **2014**, *48*, 371–389. [CrossRef]
12. Vernikovsky, V.; Metelkin, D.; Vernikovskaya, A.; Matushkin, N.; Kazansky, A.; Kadilnikov, P.; Romanova, I.; Wingate, M.; Larionov, A.; Rodionov, N. Neoproterozoic tectonic structure of the Yenisei Ridge and formation of the western margin of the Siberian craton based on new geological, paleomagnetic, and geochronological data. *Russ. Geol. Geophys.* **2016**, *57*, 47–68. [CrossRef]
13. Nozhkin, A.D.; Borisenko, A.S.; Nevolko, P.A. Stages of the Late Proterozoic magmatism and ages of gold mineralization in the Yenisei Ridge. *Russ. Geol. Geophys.* **2011**, *52*, 158–181. [CrossRef]
14. Vernikovsky, V.A.; Vernikovskaya, A.E. Tectonics and evolution of the granitoid magmatism in the Yenisei Ridge. *Russ. Geol. Geophys.* **2006**, *47*, 35–52.
15. Konstantinov, M.; Cherkasov, S.; Dankovtsev, R.; Egorkin, A. Specific crustal features of large and superlarge endogenic gold deposits (Siberia and Far East regions). *Glob. Tectonics Met.* **1999**, *7*, 143–147. [CrossRef]
16. Li, L.V. *The Olympiada Disseminated Gold-Sulfide Deposit*; KNIIGiMS: Krasnoyarsk, Russia, 2003; p. 120. (In Russian)
17. Zabiyaka, A.I.; Kurgankov, P.P.; Gusarov, Y.V.; Samkov, V.V.; Zobov, N.E. *Tectonics and Metallogeny of the Lower Angara Region*; KNIIGiMS: Krasnoyarsk, Russia, 2004; p. 322. (In Russian)
18. Serdyuk, S.S.; Komorovskiy, Y.E.; Zverev, A.I.; Oyaber, V.K.; Vlasov, V.S.; Babushkin, V.E.; Kirilenko, V.A.; Zemlyanskiy, S.A. *Models of Gold Deposits in the Yenisei Area of Siberia*; IGDGiG: Krasnoyarsk, Russia, 2010; p. 582. (In Russian)
19. Likhanov, I.I.; Reverdatto, V.V.; Sheplev, V.S.; Verschinin, A.E.; Kozlov, P.S. Contact metamorphism of Fe- and Al-rich graphitic metapelites in the Transangarian region of the Yenisey Ridge, eastern Siberia, Russia. *Lithos* **2001**, *58*, 55–80. [CrossRef]
20. Likhanov, I.I.; Reverdatto, V.V.; Kozlov, P.S.; Khiller, V.V.; Sukhorukov, V.P. Three metamorphic events in Precambrian P-T-t history of the TransangarianYenisey Ridge recorded in garnet grains in metapelites. *Petrology* **2013**, *21*, 561–578. [CrossRef]
21. Likhanov, I.; Reverdatto, V.; Kozlov, P.; Khiller, V.; Sukhorukov, V. P–T–t constraints on polymetamorphic complexes of the Yenisey Ridge, East Siberia: Implications for Neoproterozoic paleocontinental reconstructions. *J. Asian Earth Sci.* **2015**, *113*, 391–410. [CrossRef]
22. Likhanov, I.; Reverdatto, V. P–T–t constraints on the metamorphic evolution of the Transangarian Yenisei Ridge: Geodynamic and petrological implications. *Russ. Geol. Geophys.* **2014**, *55*, 299–322. [CrossRef]
23. Likhanov, I.; Reverdatto, V.; Kozlov, P. Collision-related metamorphic complexes of the Yenisei Ridge: Their evolution, ages, and exhumation rate. *Russ. Geol. Geophys.* **2011**, *52*, 1256–1269. [CrossRef]
24. Kachevsky, L.K.; Kachevskaya, G.I.; Grabovskaya, Z.M. *Geological Map of the Yenisei Ridge on a Scale of 1:500,000*; Mkrtychyan, A.K., Sherman, M.L., Eds.; Krasnoyarskgeols'emka: Krasnoyarsk, Russia, 1998. (In Russian)
25. Zvyagina, E.A. Metamorphism and gold metallogeny of the Upper Enashimo ore cluster. Master's Thesis, Siberian Federal University, Krasnoyarsk, Russia, 1989; p. 275. (In Russian).
26. Likhanov, I.; Polyansky, O.P.; Reverdatto, V.V.; Memmi, I. Evidence from Fe- and Al-rich metapelites for thrust loading in the Transangarian region of the Yenisey Ridge, eastern Siberia. *J. Metamorph. Geol.* **2004**, *22*, 743–762. [CrossRef]
27. Vernikovsky, V.A.; Vernikovskaya, A.; Kotov, A.; Sal'Nikova, E.; Kovach, V. Neoproterozoic accretionary and collisional events on the western margin of the Siberian craton: New geological and geochronological evidence from the Yenisey Ridge. *Tectonophysics* **2003**, *375*, 147–168. [CrossRef]
28. Sazonov, A.M.; Ananyev, A.A.; Poleva, T.V.; Khokhlov, A.N.; Vlasov, V.S.; Zvyagina, E.A.; Fedorova, A.V.; Tishin, P.A.; Leontyev, S.I. Gold-ore metallogeny of the Yenisey Ridge: Geological-structural provincialism, structural types of ore fields. *J. Sib. Fed. Univ. Eng. Technol.* **2010**, *4*, 371–395. (In Russian)
29. Vernikovskaya, A.E.; Vernikovsky, V.A.; Popov, N.V.; Yasenev, A.M.; Wingate, M.T.D. The oldest granitoids in the transangara region of the Yenisei Ridge: U-Th-Pb data on zircon. *Dokl. Earth Sci.* **2004**, *397*, 616–620.
30. Gibsher, N.; Tomilenko, A.; Sazonov, A.; Bul'Bak, T.; Khomenko, M.; Ryabukha, M.; Shaparenko, E.; Sil'Yanov, S.; Nekrasova, N. Ore-bearing fluids of the Eldorado gold deposit (Yenisei Ridge, Russia). *Russ. Geol. Geophys.* **2018**, *59*, 983–996. [CrossRef]
31. Yui, T.-F.; Huang, E.; Xu, J. Raman spectrum of carbonaceous material: A possible metamorphic grade indicator for low-grade metamorphic rocks. *J. Metamorph. Geol.* **1996**, *14*, 115–124. [CrossRef]
32. Baksi, A.K.; Archibald, D.A.; Farrar, E. Intercalibration of 40Ar/39Ar Dating Standards. *Chem. Geol.* **1996**, *129*, 307–324. [CrossRef]
33. Holdaway, M. Application of new experimental and garnet Margules data to the garnet-biotite geothermometer. *Am. Miner.* **2000**, *85*, 881–892. [CrossRef]
34. Henry, D.; Guidotti, C.; Thomson, J. The Ti-saturation surface for low-to-medium pressure metapeliticbiotites: Implications for geothermometry and Ti-substitution mechanism. *Am. Mineral.* **2005**, *90*, 316–328. [CrossRef]

35. Wu, C.-M.; Chen, H.-X. Revised Ti-in-biotite geothermometer for ilmenite- or rutile-bearing crustal metapelites. *Sci. Bull.* **2015**, *60*, 116–121. [CrossRef]
36. Wu, C.-M.; Zhang, J.; Ren, L.-D. Empirical Garnet-Biotite-Plagioclase-Quartz (GBPQ) Geobarometry in Medium- to High-Grade Metapelites. *J. Pet.* **2004**, *45*, 1907–1921. [CrossRef]
37. Kranidiotis, P.; MacLean, W.H. Systematics of chlorite alteration at the Phelps Dodge massive sulfide deposit, Matagami, Quebec. *Econ. Geol.* **1987**, *82*, 1898–1911. [CrossRef]
38. Jowett, E.C. Fitting iron and magnesium into the hydrothermal chlorite geothermometer. In Proceedings of the Program with Abstracts 16, A62. GAC/MAC/SEG Joint Annual Meeting, Toronto, ON, Canada, 27–29 May 1991.
39. McDowell, S.D.; Elders, W.A. Authigenic layer silicate minerals in borehole Elmore 1, Salton Sea Geothermal Field, California, USA. *Contrib. Mineral. Petrol.* **1980**, *74*, 293–310. [CrossRef]
40. Cathelineau, M.; Nieva, D. A chlorite solid solution geothermometer the Los Azufres (Mexico) geothermal system. *Contrib. Mineral. Petrol.* **1985**, *91*, 235–244. [CrossRef]
41. Bourdelle, F.; Parra, T.; Chopin, C.; Beyssac, O. A new chlorite geothermometer for diagenetic to low-grade metamorphic conditions. *Contrib. Miner. Pet.* **2013**, *165*, 723–735. [CrossRef]
42. Wiewióra, A.; Weiss, Z. Crystallochemical classifications of phyllosilicates based on the unified system of projection of chemical composition: II. The chlorite group. *Clay Miner.* **1990**, *25*, 83–92. [CrossRef]
43. Rahl, J.M.; Anderson, K.M.; Brandon, M.T.; Fassoulas, C. Raman spectroscopic carbonaceous material thermometry of low-grade metamorphic rocks: Calibration and application to tectonic exhumation in Crete, Greece. *Earth Planet. Sci. Lett.* **2005**, *240*, 339–354. [CrossRef]
44. Likhanov, I.I.; Santosh, M. The 'triple point' paradigm of aluminosilicates revisited. *Geol. J.* **2020**, *55*, 4772–4789. [CrossRef]
45. Nozhkin, A.D.; Likhanov, I.I.; Reverdatto, V.V.; Kozlov, P.S. Grenville orogeny, Late Neoproterozoic rift-related and intraplate magmatism at the western margin of the Siberian craton as geological evidence for the assembly and breakup of Rodinia. In *Proceedins of the Rodinia 2013: Supercontinental Cycles and Geodynamics Symposium, Moscaw, Russia, 20–24 May 2013*; Veselovskiy, R., Lubnina, N., Eds.; PERO Press: Moscow, Russia, 2013; p. 55.
46. Luque, F.J.; Pasteris, J.; Wopenka, B.; Rodas, M.; Barrenechea, J.F. Natural fluid-deposited graphite; mineralogical characteristics and mechanisms of formation. *Am. J. Sci.* **1998**, *298*, 471–498. [CrossRef]
47. Large, D.J.; Christy, A.G.; Fallick, A.E. Poorly crystalline carbonaceous matter in high grademetasediments: Implications of graphitization and metamorphic fluids compositions. *Contrib. Mineral. Petrol.* **1994**, *116*, 108–116. [CrossRef]
48. Petrov, V.G. *Gold Metallogeny of the Northern Yenisei Ridge*; Nauka: Novosibirsk, Russia, 1974; p. 140. (In Russian)
49. Sazonov, A.M. *Geochemistry of Gold in Metamorphic Formations*; Tomsk Polytechnical University Publishing: Tomsk, Russia, 1998; p. 166. (In Russian)